Optimization of Heat Exchanger Design Parameters for Hydrocarbon Refrigerant Systems

S. Jain and C. W. Bullard

ACRC TR-233   September 2004

For additional information:

Air Conditioning and Refrigeration Center
University of Illinois
Mechanical & Industrial Engineering Dept.
1206 West Green Street
Urbana, IL 61801

(217) 333-3115

Abstract

Hydrocarbon refrigerants (HC's) are one alternative to hydrofluorocarbons (HFC's) since they have zero ozone depletion potential and negligible global warming potential. However, due to their flammable nature, the amount of refrigerant used in systems is regulated for safety reasons.

This report presents simulation results for a 3-ton R290 (propane) air-conditioning system, and identifies the optimum heat-exchanger geometries that would minimize system charge while trying to retain the same system efficiency. An existing R410A microchannel system simulation served as the base case, and then the geometries were optimized for the R290 system, and the results were compared to the base case. The model was then analyzed for the off-design conditions, and the conclusions presented.

The optimal condenser geometry tended to have smaller port diameter and core depth with thicker webs between the ports. Also, the fins tended to be taller, thinner and more densely packed. Similar results were noted for the evaporator geometry. The optimal design reduced the combined heat exchanger charge by more than a factor of 5. The system efficiency was reduced by 3% in the process, but the loss could be recovered because the pressure drop was low enough to permit increasing the air-flow rates.

The off-design behavior of the R290 microchannel system is very different from a traditional R410A round-tube plate-fin system. Typically with the increase in ambient temperature, charge from the evaporator and the liquid line moves to the condenser. In the R290 system, because of the oil/refrigerant solubility characteristics, charge from the compressor sump also moves to the condenser.

In the microchannel systems, the heat exchangers account for only 20% of the system charge as opposed to 70% in the tube fin systems. At higher ambient temperatures, the additional charge flowing from the other components, provides the condenser with the additional ~7% charge it needs at hot ambient conditions. However, due to the small internal volume of the heat exchangers in microchannel systems, an additional 60% charge flows into the condenser, resulting in high values of subcooling, thus reducing system efficiency. One solution to this problem would be to install a receiver at the outlet from the condenser, to retain high levels of efficiency across a wide range of operating conditions.

Table of Contents

List of Figures

List of Tables

Nomenclature

Variables

T:	temperature (°C)
A:	area (m^2)
P:	pressure (kPa)
G:	mass flux (kg /m^2-s)
m_{dot} :	mass flow rate (kg / sec)
Q:	capacity (kW)
W:	compressor work (kW)
V:	volume (m^3)
V_{dot}:	volumetric flow rate (m^3 / sec)
D:	diameter (mm)
COP:	coefficient of performance (-)
NTU:	number of thermal units (-)
SHR:	sensible heat ratio (-)
x:	dryness fraction
v:	specific volume (m^3 / kg)
t:	thickness (mm)
h:	enthalpy (kJ / kg)
s:	entropy (kJ / kg-K)

Greek

η:	efficiency (-)
ρ:	density (kg/m^3)
ε:	effectiveness (-)

Subscripts

air:	air side parameter
ref:	refrigerant side parameter
cond:	condenser parameter
evap:	evaporator parameter
amb:	ambient conditions
sat:	saturated conditions
sup:	superheat
sub:	subcooling
sys:	system
cyc:	cycle
app:	approach
fflow:	free flow area
fin:	fin parameter
port:	microchannel port parameter
fan:	condenser fan parameter
web:	microchannel tube web parameter

Chapter 1: Introduction

In this particular part of the project, we focus on microchannel heat exchangers, and try to analyze their benefits in applications using hydrocarbon (propane and butane) refrigerant systems.

Hydrocarbon fluids are natural refrigerants and are generally considered environmentally benign. They have negligible GWP (global warming potential) and zero ODP (ozone depletion potential). Propane for example is compatible with most common metals and can therefore be used with most of the components and compressors already in use. It is compatible with most common plastics as well. However, as Granryd [1] pointed out, flammability is an issue with the hydrocarbon refrigerants and various standards have been set, which limit the amount of hydrocarbon charge as a refrigerant in a system. Hence in most of the cases these refrigerants considered for use only in low capacity (<1 ton) applications.

This project explores the potential for microchannel heat exchangers to minimize charge in a hydrocarbon refrigerant system, with only a small COP penalty. Using microchannels helps in reducing system charge as reported by Hoehne [2], and would keep the hydrocarbon charge within the specified flammability limits. Also, flat multi-port tubes have lower airside pressure drop, higher refrigerant side area and allow for greater airside surface area within a given volume. The following analysis quantifies the tradeoffs between efficiency and charge, and identifies proper charging strategies that will ensure acceptable off-design performance.

Section 2 of the report describes the different geometric parameters in microchannel heat exchangers. Section 3 presents the details of the simulation model used in analyzing the system. We begin by focusing on one of the components of the system, the condenser. Since there are no microchannel heat exchangers built specifically for R290 applications, we start with a prototype R410A three-ton residential air-conditioning condenser, manufactured by Modine, as our base case. [3]

The next step, described in Section 4, is to modify the condenser tube and fin parameters so as to achieve minimum charge. At the same time, we would want to ensure that we do not lose out on the system efficiency. Hence, the goal is to optimize the geometry so as to reduce the charge while trying to achieve higher or the same efficiency than the base case. Once the condenser geometry is optimized, the same process is followed for the evaporator, and eventually for the system, which is presented in Section 5. Finally in Section 6, system behavior at off-design conditions is contrasted with that of conventional round tube/ plate fin heat exchangers.

Appendix A describes the individual steps taken while modifying the model, to convert it such that we have the geometry variables as the outputs. Appendix B presents the detailed systems efficiency and refrigerant charge plots obtained by varying the fin pitch. The R410A and the R290 round tube-plate fin systems are compared in Appendix C. This section describes the difference observed during the off-design operation of a round tube-fin system using these refrigerants. Microchannel and round tube-plate fin R410A systems are compared in Appendix D. The section gives a detailed account of the off-design characteristics of these systems. Appendix E presents the effects of varying the length of the liquid line during off-design conditions on the system parameters, while Appendix F gives a detailed analysis of the effect of using different oil/refrigerant combinations in a R290 system.

Chapter 2: Microchannel heat exchangers

Microchannels have tube and fin geometries quite from the standard round tube-fin heat exchangers. Hence, before trying to build a simulation model, we discuss the various geometry parameters involved briefly, as shown below in the Figures 2.1 and 2.2.
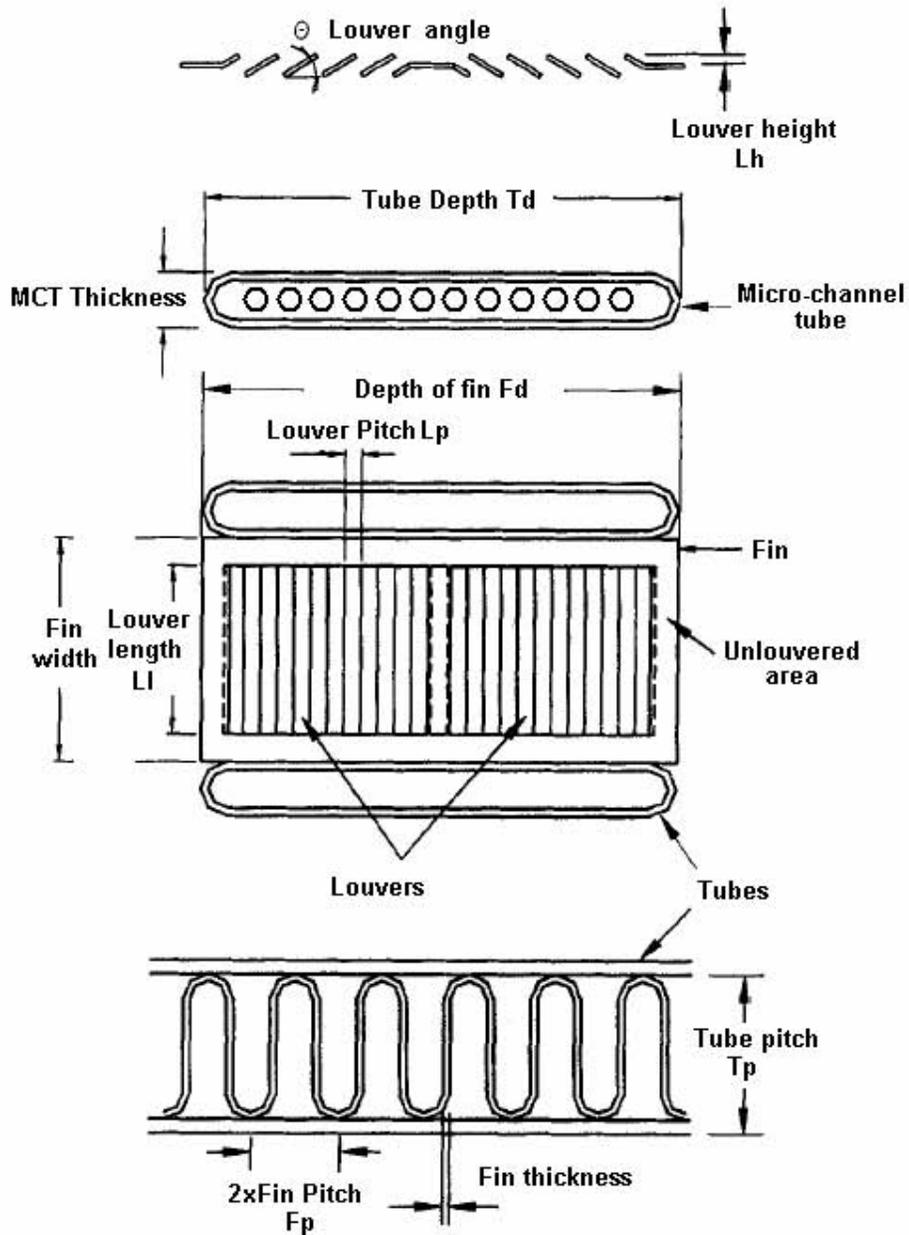
Figure 2.1. Microchannel heat exchanger geometry parameters
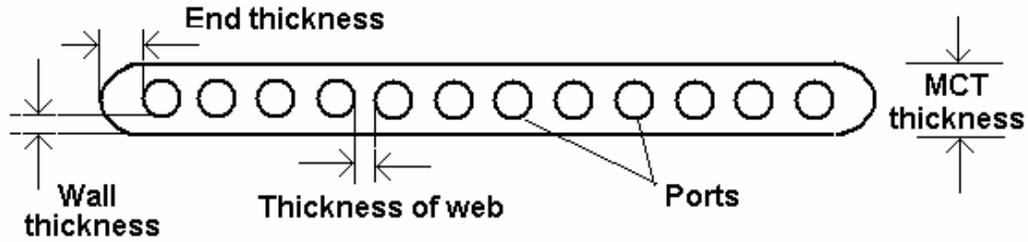
Figure 2.2 Microchannel tube geometry parameters

One of the most important correlations used in the model is for the air-side heat transfer coefficient for the louvered fin geometry given by the following equation, developed by Chang and Wang [4].

$$j_{cw} := Re_{Lp}^{-0.49} \cdot \left[\frac{\theta}{90}\right]^{0.27} \cdot \left[\frac{Fp}{Lp}\right]^{-0.14} \cdot \left[\frac{Width_{fin}}{Lp}\right]^{-0.29} \cdot \left[\frac{Td}{Lp}\right]^{-0.23} \cdot \left[\frac{LL}{Lp}\right]^{0.68} \cdot \left[\frac{Tp}{Lp}\right]^{-0.28} \cdot \left[\frac{Thick_{fin}}{Lp}\right]^{-0.05}$$

$$h_{airCW} := G_{max} \cdot cp_{air} \cdot Pr^{-0.667} \cdot j_{cw}$$

Similarly, the refrigerant side heat transfer coefficient is given by the correlation by Dobson and Chato [5]. The main conclusions that can be derived from these correlations are as follows.

- Increasing the port diameter, results in the decrease of the air-side heat transfer coefficient. Increasing the port diameter, increases the tube depth (T_d) and the tube pitch (T_p), both of which are inversely proportional to the heat transfer coefficient, and hence it decreases.

- Increasing the number of ports (keeping all the other parameters constant), increases the tube depth thus resulting in a decrease in the heat transfer coefficient.

- Increasing the fin thickness (t_{fin}) reduces the air flow area (A_{fflow}), thus increasing the maximum air flux (G_{max}), and hence increases the heat transfer coefficient.

- Increasing the fin width ($Width_{fin}$), increases the tube pitch, thus reducing the heat transfer coefficient.

- Increasing the fin density reduces the air flow area, thus increasing the maximum air flux, hence increasing the heat transfer coefficient.

- Increasing the port diameter, results in the decrease of the refrigerant side heat transfer coefficient.

Thus changing any of these parameters has an effect on the heat transfer coefficient and hence the system efficiency. Moreover, any change in the refrigerant side volume would result in a change in the refrigerant charge.

Our aim is to optimize these heat exchanger geometry parameters. Given the fact that the propane and other hydrocarbon refrigerants are flammable, we would want keep the charge in the system to a minimum, while at the same time, try to keep the efficiency as high as possible.

3

Chapter 3: The simulation model

A finite volume approach is adopted to model the actual physics in the heat exchanger geometries. The whole heat exchanger is divided into small elements along the refrigerant flow direction. Each finite volume is assumed to be a cross-flow heat exchanger and solved for the amount of heat transfer occurring between the refrigerant and the air. Within each element the fluid properties are assumed constant and pressure drop calculated after heat transfer calculations have been done. The outlet refrigerant state from one element becomes inlet for the next. If an element is encountered in which the refrigerant changes its phase (transition element) it is split into two sub-elements where each one is solved separately. The amount of heat transfer from refrigerant to air is calculated using the ε-NTU method (Incropera & DeWitt [6]).

Various correlations are used in the model. Single-phase refrigerant side heat transfer coefficient and pressure drop are calculated using the correlations by Gnielinski and Churchill [7], respectively, while the two-phase condensation is calculated using the Dobson and Chato (1998) correlation. The refrigerant side 2-phase pressure drop is obtained using the correlation from Souza and Pimenta [8]. Air-side heat transfer coefficient and pressure drop for the louvered fins used in the model were obtained from correlations by Wang and Chang [9].

For the evaporator, the same finite volume modeling approach is used, but modified to express the total heat transfer as the sum of latent and sensible components using the total enthalpy driving potential method. A wet element is further divided into small elements in the airflow direction to separate the latent and sensible heat loads using trapezoidal finite difference method (Song and Bullard, [10]). The two-phase refrigerant heat transfer coefficient is obtained from Wattelet and Chato [11] correlation. The refrigerant side pressure drop and the air-side heat transfer and pressure drop correlations are the same as the condenser module.

In the simulations that follow, we assume that the fins are made of aluminum with a given conductivity. We also assume that a few of the input parameters are constant. The fin pitch for the condenser is held constant at 1 mm, while that for the evaporator as 1.4 mm. The fin thickness is assumed to be approximately 0.1 mm. Similarly the louver pitch is also fixed at 1 mm.

The baseline prototype microchannel condenser had a three-pass configuration. The first step is to reduce the three-pass configuration to a single pass system, for two reasons. First it is easier to identify the effects of individual parameters in a single pass system, and second, such circuiting is more suitable for reversible heat pump systems because they minimize the potential for maldistribution in the intermediate headers in evaporator mode. The system model is depicted in Figure 3.1, with the inputs on the left hand side and the outputs on the right hand side. Initially, all the geometry variables were supplied to the model, along with the design point condition of meeting 10.5 kW capacity (at $T_{amb} = 35°C$), with ΔT_{sup} and ΔT_{sub} being 5°C. Variables like ΔT_{sat}, A_{face}, Q_{cond}, and the system COP were calculated.
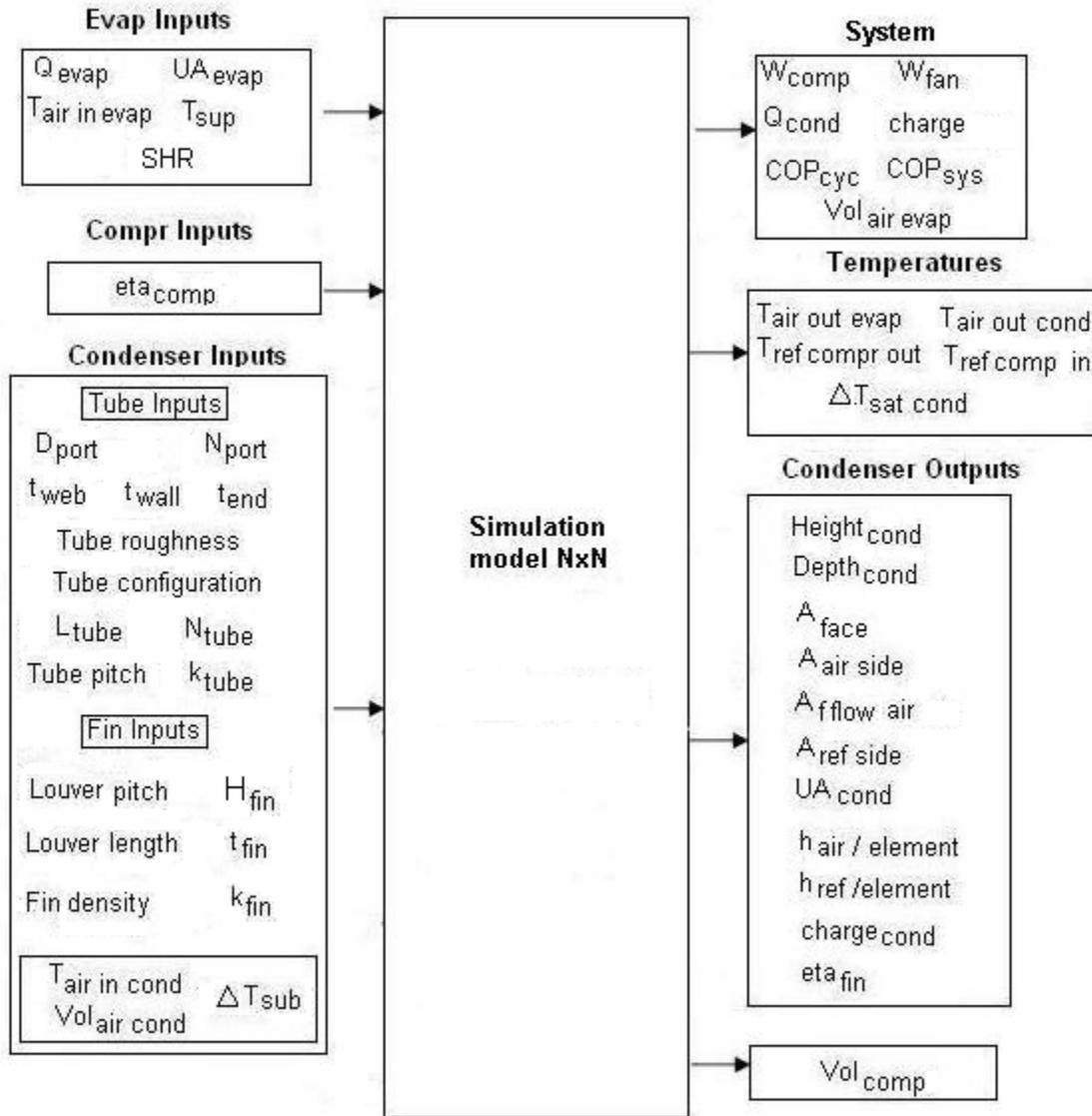
Figure 3.1 Simulation model, with the initial inputs

The compressor efficiency (eta_{compr}) was assumed to be a linear function of the pressure ratio, while the evaporator and condenser fans were assumed to be 20% efficient. The initial model can also be represented as shown in Figure 3.2.
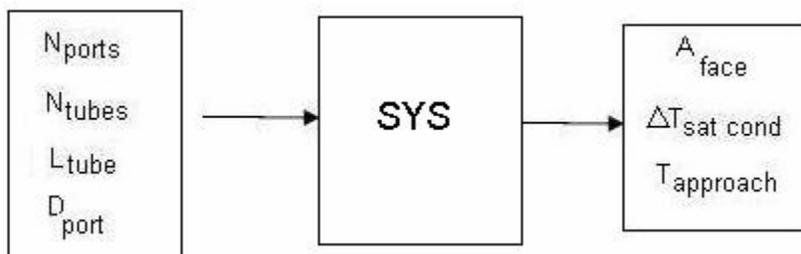
Figure 3.2. Simple representation of NxN model

5

As is shown in Figure 3.2, the simulation model takes the geometry parameters as input, and then calculates the saturation pressure drop and the approach temperature difference. We would want to set the model up in a manner, so that the latter values are set as input, and instead we calculate the geometry parameters like the number of tubes, number of ports and length of tubes as outputs. That would allow us to modify other geometric parameters and still be able to satisfy the same design performance constraints. The simulation model was modified accordingly (Appendix A) and can be represented by Figure 3.3 in its final form.
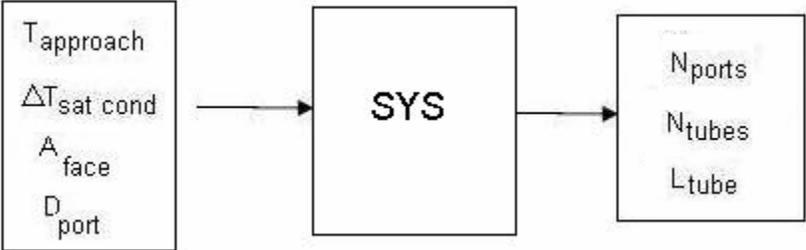
Figure 3.3. Switching between ΔT_{app} and N_{ports}

Chapter 4: Optimizing the heat exchanger geometry

Once the variables have been switched, other geometry parameters are allowed to vary and thus the optimum geometry is calculated. The refrigerant side pressure drop (ΔT_{sat}) was assumed to be 1°C in the simulation model. Saturation temperature drops of less than 0.5°C would require more condenser tubes and correspondingly higher manufacturing costs. It would also increase the risk of maldistribution of charge as header pressure drop may not be negligible relative to that in the tubes. Similarly, values of more than 1.5°C, would result in significant pressure drop, leading to higher compressor work and thus lower system COP, hence the choice of 1°C is justified. Microchannel tubes in the heat exchangers can be serpentined to change the aspect ratio of the core, and hence the tube length would not necessarily indicate the heat exchanger's width.

In the model ΔT_{app} is assumed to be 2°C. Taking lower values would result in the addition to the core depth and hence to the manufacturing cost. Similarly, values higher than 2°C would introduce a substantial efficiency penalty. Later on, in the analysis this constraint has been removed and different values of ΔT_{app} have been used. For purposes of this analysis the approach temperature difference for this purpose is defined differently – in terms of the approach of air and refrigerant temperatures in the midpoint of the crossflow condenser – a crude surrogate for the tradeoff between heat exchanger material cost and the operating energy cost.

4.1 Varying port diameter

The system has three constants as the input, the face area A_{face}, the approach temperature (ΔT_{app}) and the refrigerant pressure drop (represented by ΔT_{sat}), while it calculates the three geometry parameters N_{tubes}, N_{ports} and L_{tubes}. This step involves varying the port diameter and analyzing its effect on the system parameters and condenser charge.

Increasing the port diameter would increase the condenser depth. However, to maintain the ΔT_{app}, the number of ports go down. Increasing the diameter would also result in a decrease in the pressure drop as it is inversely proportional to refrigerant mass flux. So, to match the $\Delta T_{sat} = 1$°C condition, the length of tubes would increase. This would lead to a reduction in the height of the condenser since the face area is being held constant, and would eventually lead to a reduction in the number of tubes. It is observed that increasing the port diameter by a factor of *three* increases the refrigerant condenser volume (and the charge) by almost a factor of *four* (Figure 4.1). However, the above-mentioned ΔT_{app} constraint maintains the $T_{sat,dis}$ to almost a constant value and hence fixes the compressor work, thus allowing little variation in the system COP.
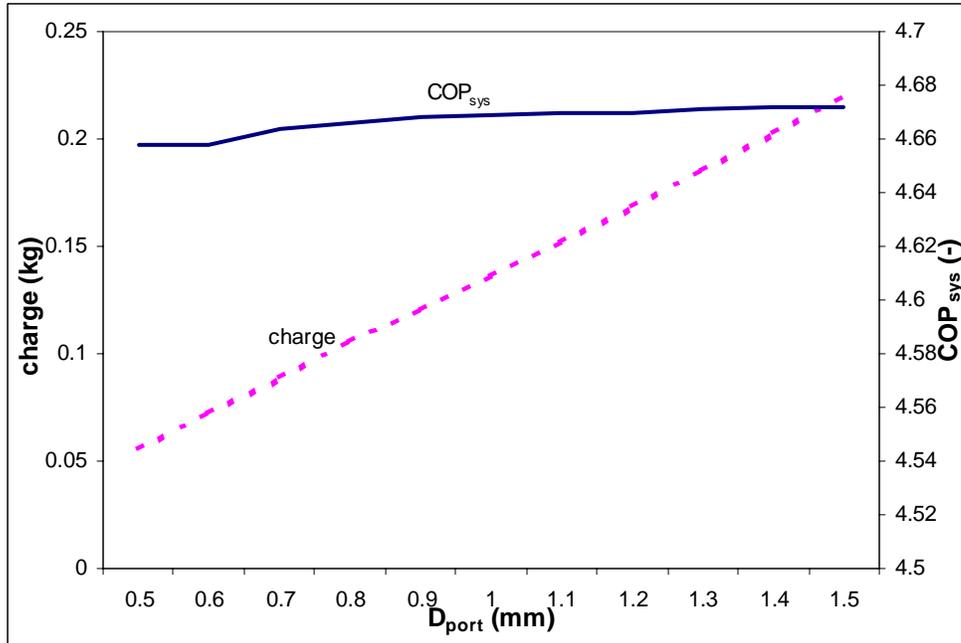
Figure 4.1. System COP and condenser charge as a function of port diameter

Increasing the port diameter reduces both the refrigerant side and air-side heat transfer coefficients. Therefore to achieve the same condenser capacity the refrigerant side temperature difference ΔT_{ref} increases. Increasing the port diameter would also increase the refrigerant side volume and hence the charge, as is predicted by the model. The reasoning suggests that the system would have the minimum condenser charge for the smallest port diameter. However, there is a manufacturing limit on the size of the ports, and hence we choose the smallest possible ($D_{port} = 0.5$ mm).

4.2 Round versus square ports

From the manufacturing point of view, it has been observed that square ports are easier to extrude and they minimize the amount of material needed for a given flow area. Hence, most of the microchannel heat exchangers in the market today have square or rectangular ports. As part of our analysis, we also consider the effect of shape of the ports on the charge in the condenser. For a given port diameter, a circle would have a smaller area than a square having a side equal to the port diameter, and hence the square ports will hold more charge. For a port diameter of 0.5 mm, the charge for the round ports is around 12% lower than that for the square ports, and using round ports would be advisable for charge reduction.

4.3 Varying web thickness between microchannel ports

Increasing the web thickness forces the number of ports to decrease, so as to maintain the condenser depth and hence the fixed ΔT_{app} condition. Since the number of ports decreases, the refrigerant side volume and the charge also decrease. Hence theoretically, we would want to have to the maximum possible web thickness (T_{web}) between the microchannel ports, so as to minimize the charge. However, reduction in refrigerant side heat transfer surface

8

would mean higher compressor discharge saturation temperature to reject the required amount of heat rejection. This would lead to an increase in compressor work, and hence a drop in system COP, as is shown in Figure 4.2.
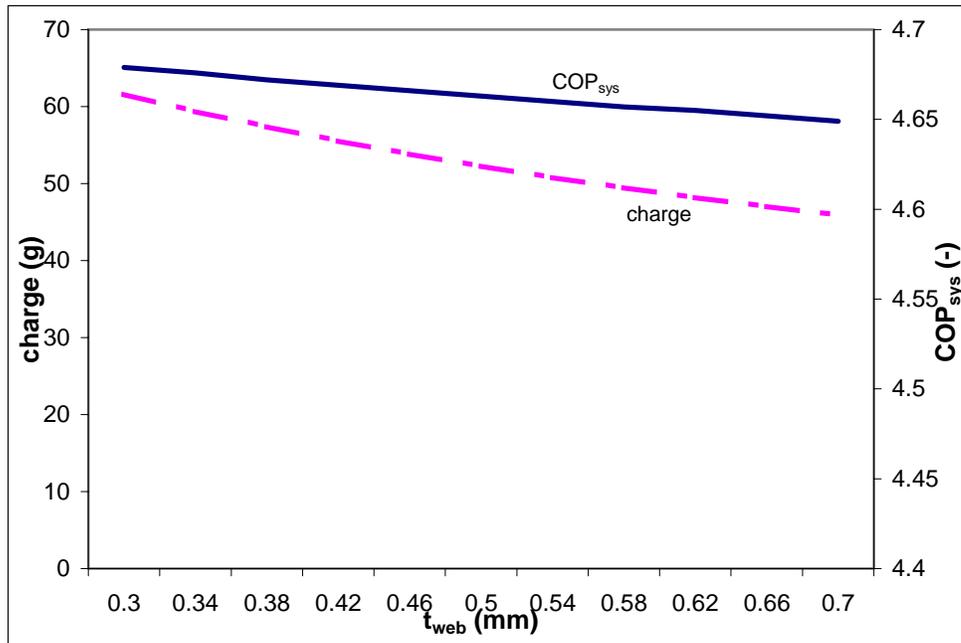
Figure 4.2 System COP and condenser charge as a function of web thickness

4.4 Varying wall thickness (t_{wall})

Increasing the wall thickness increases the microchannel tube thickness Then with fin height held constant, the number of tubes must be reduced slightly to keep the face area constant, since the tube length is being held almost constant by the ΔT_{sat} constraint. This requires a slight increase in the number of ports per tube so as to match the ΔT_{app} constraint. The refrigerant side volume remains fairly unaffected and hence the charge doesn't change, and neither does the COP.

4.5 Varying microchannel fin height

Increasing the fin height would result in lowering the number of tubes to maintain the constant face area. Reducing the number of tubes would lead to an increase in the refrigerant mass flux, and the pressure drop would increase. To maintain the $\Delta T_{sat} = 1°C$ condition, the tube length would go down. However to keep the face area constant, the height of the condenser increases to compensate for the reduction in condenser width. These effects would reduce the refrigerant side area and volume and ultimately the condenser charge.

Increasing the fin height results in the shifting of material from the tubes to the fins. This allows the air-side free-flow area to increase slightly, which results in reduction in the air side velocity. However, the pressure drop over the fins exceeds that over the tubes, and hence the overall pressure drop increases, which leads to an increase in the condenser fan power. Also, with the increase in fin height, the fin efficiency decreases. With an increase in the fin height from 6 to 18 mm, the fin efficiency is reduced by almost 15%. . This leads to an increase in the compressor discharge (condenser inlet) pressure, leading to an increase in the compressor work. These add up to an increase in the total work, and hence the system COP falls, as can be seen in Figure 4.3.
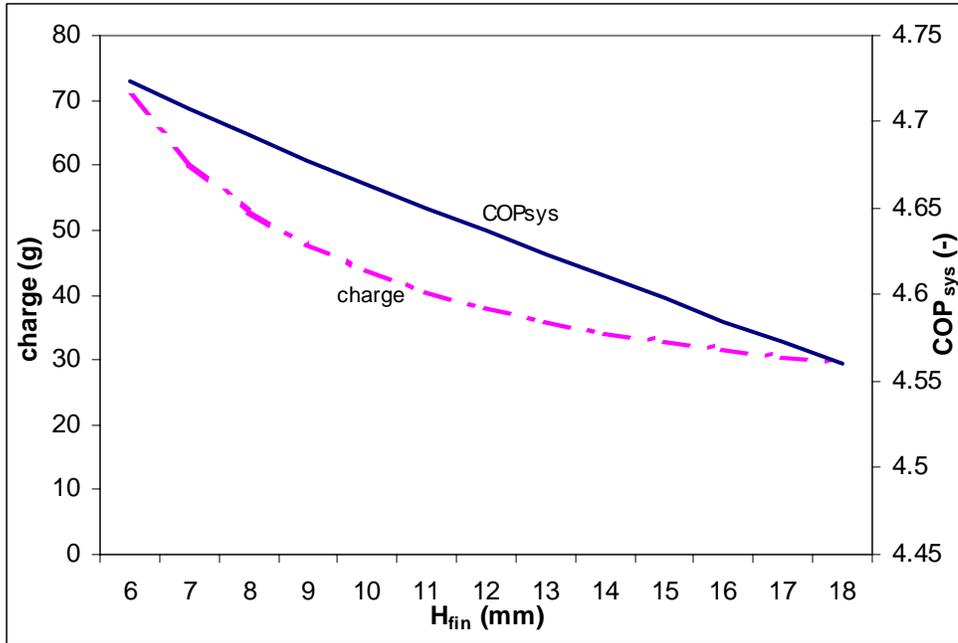
Figure 4.3. Variation of condenser charge and system COP with condenser fin height

4.6 Varying fin thickness

Another parameter that had been fixed in the original simulation was the condenser fin thickness. The next step involves removing this constraint and finding the effect of fin thickness on system performance. The face area was held constant along with the volumetric flow rate, and the fin thickness was allowed to vary from 0.06 mm to 0.15 mm. The fin spacing (the center to center distance between the fins) was kept constant at 0.09 mm, which ensured that fouling did not occur. Reducing the fin thickness allows us to pack more fins in a given area, thus increasing the fin density, which eventually leads to an increase in the air-side heat transfer area.

This allows us to shift condenser surface area from tubes to fins, and hence leads to further charge reduction. Increasing the air-side area also lets the condenser depth be reduced, which leads to a reduction in the number of ports per tube, and hence in the condenser charge. However, increasing the fin density would reduce the free flow area, thus increasing the maximum velocity. The increased velocity, by itself, would result in an increase in the condenser fan work and negatively affect the system COP, thus offsetting the effect of the thinner core, as shown in Figure 4.4.
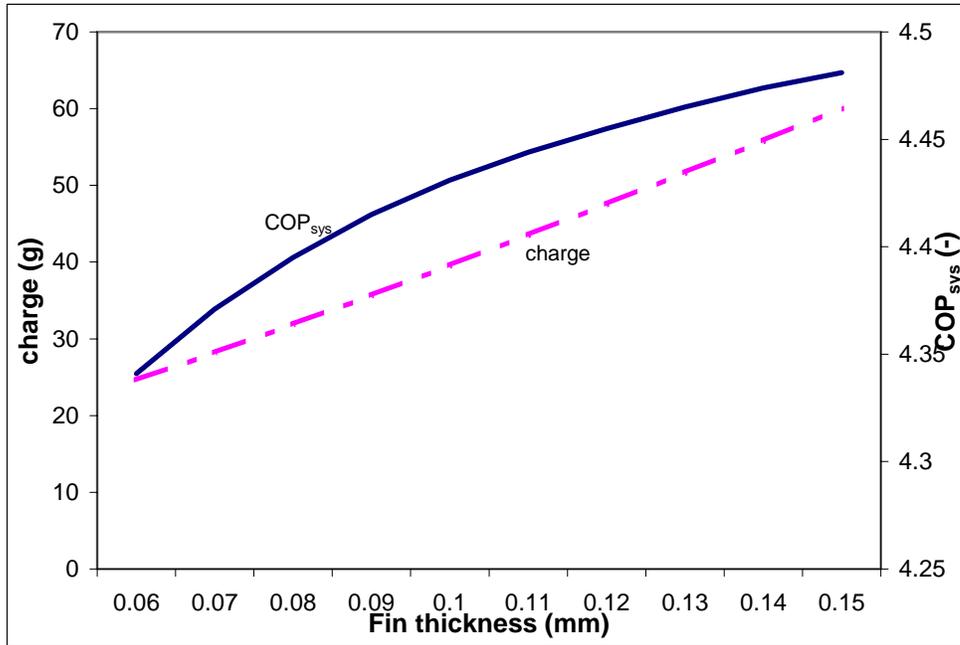
Figure 4.4. Variation of condenser charge and system COP with condenser fin thickness

Varying the fin pitch while keeping the fin thickness constant gives a similar kind of result. Reducing the fin pitch helps reduce the condenser charge, but the system efficiency goes down simultaneously. (Appendix B)

4.7 Varying condenser air flow rate

In the preceding analyses the volumetric flow rate of air over the condenser was kept constant at 2800 cfm (approximately 1.32 m^3/s). The next step involved analyzing the effect of varying flow rate on both the geometric parameters and the condenser charge and system COP. While keeping the same ΔT_{app}, increasing the air flow rate would reduce the discharge saturation temperature from the compressor, thus reducing compressor work, and increasing the system COP.

However, increasing the volumetric flow rate also increases the condenser fan work, and beyond a particular velocity the effect on the COP due to the reduced compressor work is outweighed by the more than linear increase in the condenser fan work. (Figure 4.5)
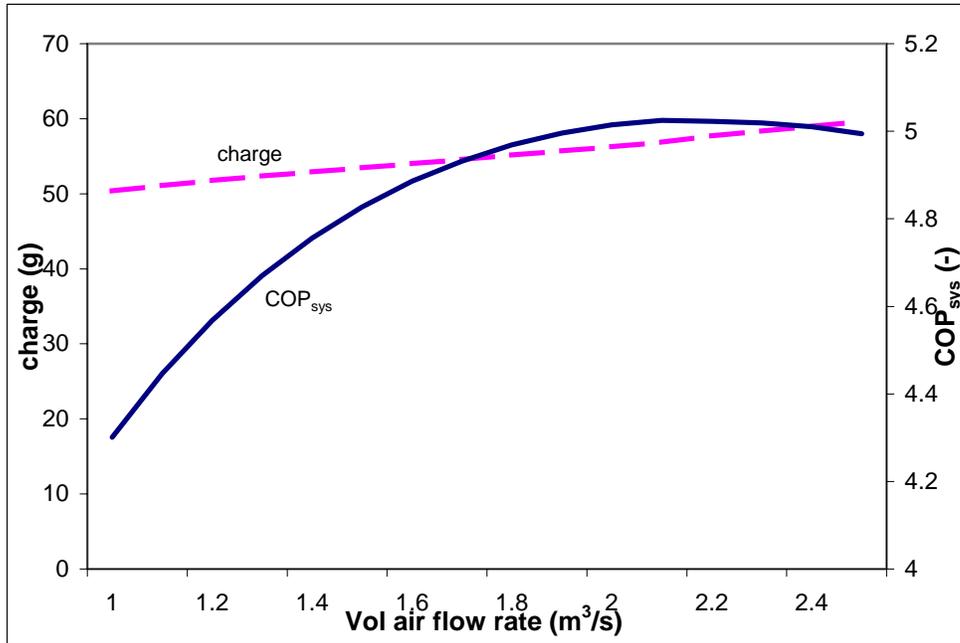
Figure 4.5. Variation of condenser charge and system COP with condenser volumetric air flow rate

With the increase in the air-flow rate from 1.2 to 1.8 m^3/s, the system COP increases by almost 5% due to the reduction in condensing temperature, despite the increase in condenser fan power. The approach temperature difference is held constant, but the savings in compressor power permits a marginal increase in the condenser depth from 10.8 to 11.2 mm and a corresponding increase in the refrigerant volume and condenser charge (~3%).

4.8 Varying condenser depth

Up to this point, the approach temperature difference was being supplied as an input to the simulation model. Fixing ΔT_{app} resulted in fixing the compressor discharge pressure, which fixed the compressor work, thus keeping the COP almost constant. By allowing the approach temperature difference to vary, we can notice a variation in the system COP. Since the approach temperature difference depends directly on condenser depth, we run the simulation model while supplying several values of depth. The face area and the refrigerant side pressure drop are kept constant, as was in all the previous cases, and the effects on ΔT_{app} are monitored.

It has already been pointed out that, to reduce the condenser refrigerant charge, using the smallest possible port diameter gives the best results. So, in this case, we fix the port diameter as 0.5 mm and begin the analysis by increasing the condenser depth by increasing the number of ports, while keeping the web thickness constant. Increasing the condenser depth, by increasing the number of ports causes the approach temperature difference to decrease, since both the refrigerant and air-side areas increase.

The reduction in ΔT_{app} lowers the compressor discharge saturation temperature, thus increasing system COP. Increasing the condenser depth, however, also increases the fan power, and eventually the system COP curve flattens out, as is shown in Figure 4.6.
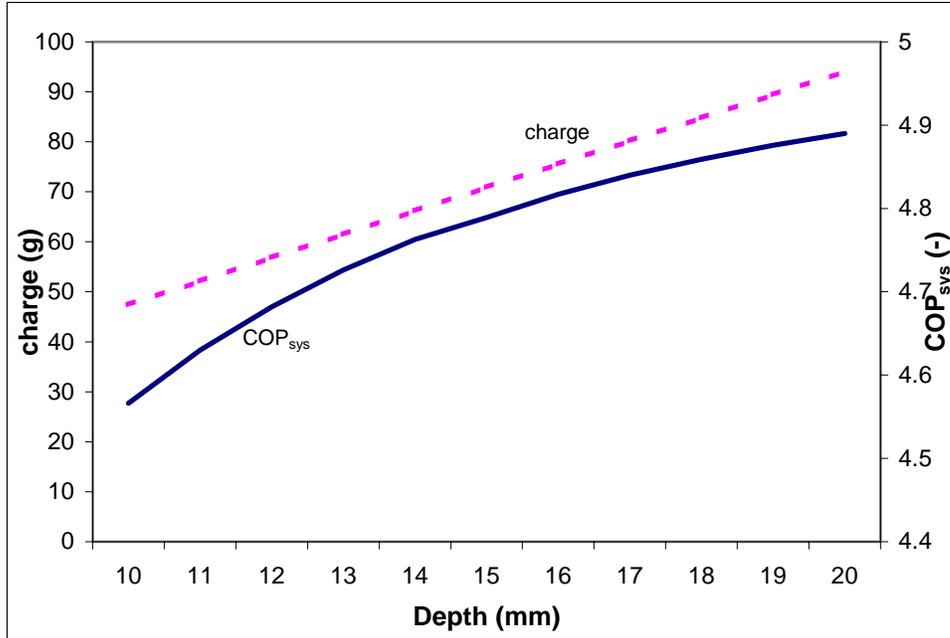
Figure 4.6. Variation of condenser charge and system COP with condenser depth

Although increasing the condenser depth in this manner increases the COP, the refrigerant charge also increases due to the increase in the number of ports. However, we can also increase the condenser depth by increasing the web thickness (T_{web}) instead of adding more ports, keeping the refrigerant charge low, as described in the following section.

4.9 Varying condenser depth (allowing T_{web} to vary)

As shown in the previous section, the system COP could be increased, by increasing the condenser depth. However, this results in additional microchannel ports, and hence the refrigerant charge increases. Hence, to obtain a COP gain, while keeping the charge constant, the condenser depth is increased, by increasing the web thickness. Figure 4.7 shows the variation in the system COP and the condenser charge with varying depth, while the number of ports is being held constant. Since the number of ports and port diameter remain constant, the refrigerant side volume does not vary, and the condenser remains almost constant.
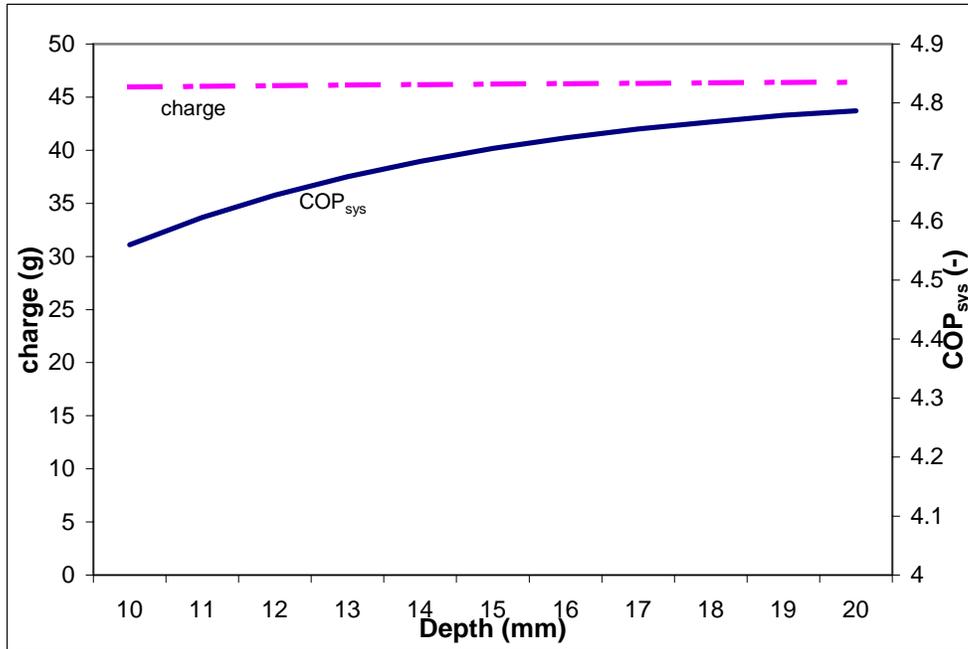
Figure 4.7. Variation of condenser charge and system COP with condenser depth (T_{web} increasing)

4.10 Varying condenser face area

In the preceding analysis, we had fixed the condenser face area and had tried to optimize other geometric parameters under the given constraints. The next step involves finding the effect on the system charge and COP while the face area is allowed to vary. Ideally, the system would try to have the maximum possible face area, so as to achieve the highest COP. In our case, we allow the face area to vary from 0.7 to 1.8 m^2. The refrigerant side pressure drop (ΔT_{sat}) and the approach temperature (ΔT_{app}) are held constant at 1°C and 2°C respectively.

First the volumetric flow rate is also kept constant at 2800 cfm or 1.3 m^3/sec. With an increase in the face area, the face velocity decreases, thus decreasing the condenser fan work and increasing the system COP. With the decrease in the face velocity, the air-side heat transfer coefficient decreases, and to offset this loss, the total tube and fin areas increase. The increase in the tube area is accompanied by an increase in the refrigerant side volume and hence in the condenser charge, since the web thickness is being held constant at this point.

The next set of calculations are done while holding the face velocity constant at 1.5 m/sec, while the face area is allowed to change. Increasing the face area in this manner would increase the volumetric air flow rate, which in turn would lower the compressor discharge saturation temperature. Since ΔT_{app} is held constant, the compressor power is reduced and the system COP increased. However, increasing the volumetric flow rate causes the condenser fan work to increase linearly, so the system COP curve flattens as we keep on adding the condenser area, as is shown in Figure 4.8. At the same time, increasing face area would mean adding more tubes, thus increasing the condenser charge.
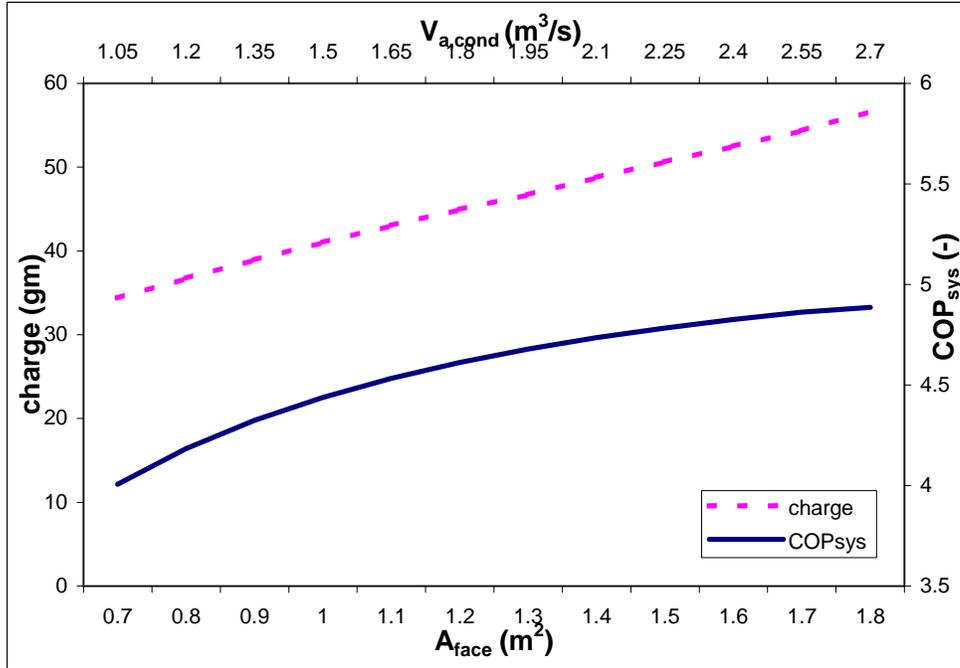
Figure 4.8 Variation of condenser charge and system COP with varying condenser face area while keeping the face velocity constant

We have analyzed most of the fin and geometry parameters for the condenser, and before moving on to the evaporator, the results are summarized as follows. With the refrigerant side pressure drop (ΔT_{sat}) and the approach temperature difference (ΔT_{app}) being held constant at 1°C and 2°C respectively, the basic conclusions are as follows.

- Reducing the port diameter (to one-third the original value) helps reducing the charge four times. The size of the port diameter has been reduced to the manufacturing limit.

- For a given port diameter, the round ports have around 10-12% less condenser charge than the square ports.

- Doubling the fin height results in the condenser charge reduced by almost 40%. However, the system COP also falls due to an increase in the compressor as well as fan power.

- Increasing the condenser depth helps lower the ΔT_{app}, which in turn reduces the compressor work and improves COP. For the same number of ports (and thus keeping charge constant), we can increase the condenser depth by increasing the web thickness between the ports and thus have a high COP with a low condenser charge.

- Increasing the air flow rate (from 1 to 2 m^3/s) reduces the compressor work and discharge pressure, thus increasing the system COP by almost 11%.

At this point, the condenser parameters have been optimized simultaneously to meet the minimal charge requirements. Since many values have changed significantly compared to the original base case, and are presented in the following table.

In both the cases, the louver angle is kept constant at 27°, while the microchannel wall and end thickness is 0.4 mm. Initially, the face area and air-flow rate are fixed as 1.4 m^2 and 2800 cfm. All other geometric variables were allowed to vary, and finally the face area and flow rate constraint was released. The resulting optimized geometry and air-flow rate are shown in Table 1.

Table 1 Condenser parameters for the base case and optimized geometry

	Base Case	Optimized geometry
Port diameter (mm)	1.28	0.5
Number of ports	12	9
Condenser depth (mm)	21	17
Number of tubes	74	93
Web thickness (mm)	0.42	1.4.5
Fin height (mm)	7.92	11
Fin thickness (mm)	0.1	0.08
Fin pitch (mm)	1	1.0
Condenser width (m)	1.85	1.6
Air side area (m^2)	49.3	43.2
Air flow rate (m^3/s)	**1.3**	**1.6**
ΔT_{app} (°C)	**0.988**	**0.878**
Charge	**303**	**45**
System COP	**4.85**	**4.85**

Through this optimization process the charge in the condenser was brought down from 313 gm to only 42 gm, i.e. a reduction of more than 7 times. Recall that these figures refer only to the charge inside the tubes; the amount in the headers will depend on details of header design. The charge in the condenser could be reduced further, but the efficiency of the system would decrease at a faster rate, so the parameters shown in the table are chosen. Basically, the optimized geometry tends to have smaller port diameter and core depth, while having thicker webs between the ports. Also, the volumetric flow rate was increased from 1.3 to 1.6 m^3/s, which helped increase the system COP to the original base case value of 4.85, without adding any additional refrigerant charge. If a volumetric flow rate of 1.3 was used fro the optimized geometry the system COP was observed to be 4.72. This means that by optimizing the geometry parameters while keeping the face area and the volumetric air-flow rate as constant the condenser charge could be reduced by almost 7 times, while registering a 2.5% drop in the system COP.

These results are also presented graphically in Figure 4.9. Each step is represented by a point on the plot, showing the tradeoff between system COP and charge, by changing the indicated parameter. The biggest drop in the charge is due to the reduction in port diameter. Using round ports, increasing web thickness, increasing fin height and lowering fin pitch further reduce the charge, but at the expense of efficiency. Increasing the volumetric flow rate and the condenser depth however allow us to improve system efficiency while keeping the charge constant.
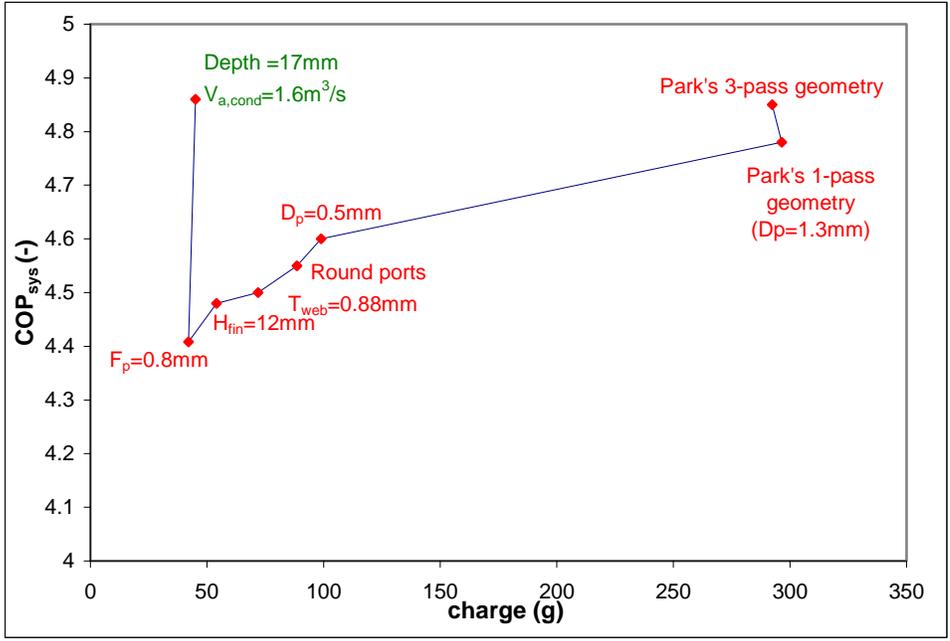
Figure 4.9 System COP and charge trade-off, by changing different condenser parameters

Chapter 5: Other components

5.1 Varying evaporator parameters

Once we have achieved the charge minimization for the condenser, we move on to the other components, namely the compressor and the evaporator. Since we do not have too many liberties with the geometry parameters in the compressor, we focus on the evaporator. The evaporator used in the original system was a tube-fin type, with a face area of 0.34 m^2, and a face velocity of 1.64 m/s [3]. Using this data, and supplementing it with typical values for the geometry parameters in a microchannel evaporator, we build a simulation model for a evaporator prototype, which has the same face area and face velocity as our tube-fin base case. The fin height and pitch are taken initially as 8.8 and 1.4 mm (to facilitate condensate drainage) respectively, while the louver length and louver pitch are assumed to be 7.16 and 1.7 mm respectively [12]. The fin thickness is chosen as 0.1 mm while the louver angle is 27 degrees. Next, we go through the same steps of switching between the variables, as we did in case of the condenser. Eventually for the NxN model, we fix the face area (A_{face}), the refrigerant side pressure drop (ΔT_{sat}) and the approach temperature difference (ΔT_{app}) as an input, and try to find the geometry parameters L_{tubes}, N_{tubes} and N_{ports}. Next, as we did in the previous case, we do a parametric analysis for the port diameter (D_{port}), and try to find the optimum value.

For the evaporator we constrain the refrigerant side pressure drop (ΔT_{sat}) to 1°C, and the approach temperature difference (ΔT_{app}) to 2°C, the same values that we took for the initial analysis of the condenser.

The results obtained are similar to the condenser case. Reducing the port diameter, from 1.6 mm to 0.5mm helps reduce charge by a factor of 3 (from **98** to **34** gm), due to the reduction in the refrigerant-side volume. The system COP also improves by around 2%, by opting for the smaller diameter ports. Most of the increase in COP is due to the reduction in the evaporator fan power. Reducing the port diameter helps in reducing the evaporator depth and thus the evaporator fan power.

Like we did in case of the condenser, we next try to reduce the charge further by reducing the number of ports and increasing the web thickness. Replacing refrigerant with metal would allow us to maintain almost the same core depth, so as to meet the approach temperature constraint.

The optimized geometry of the evaporator is presented in Table 2. Just as in the case of the condenser, the charge in the evaporator could be reduced further, but the efficiency of the system would decrease more sharply, so the parameters shown in the table are chosen for further analysis. The optimized geometry again tends to have smaller port diameter, while having thicker webs between the ports, and taller fins.

Table 2 Evaporator parameters for the optimized geometry

Parameters	Optimized geometry
Port diameter (mm)	0.5
Number of ports	24
Evaporator depth (mm)	40.8
Number of tubes	32
Web thickness (mm)	0.8
Fin height (mm)	11
Fin thickness (mm)	0.08
Fin pitch (mm)	1.4
Evaporator width (m)	0.54
Air flow rate (m^3/s)	**1.4**
ΔT_{app} (°C)	**0.88**
Charge	**23**
System COP	**4.65**

5.2 Compressor charge calculation

The next step involves the calculation of charge in the compressor. The refrigerant charge in the compressor comprises of the charge in the low-side shell, plus the charge dissolved in the lubricating oil in the compressor sump, which is assumed to be on the low pressure side. In our case, we assume the oil to be ICI POE 32, which is often used for propane systems. The solubility and liquid density data for the oil-propane mixture is taken from a presentation by Seeton [8]. The compressor shell volume is assumed to be 2183 cc, which is the volume of R410A compressor in an equivalent 3-ton R410A compressor [9]. Similarly, the mass of oil inside the compressor is also assumed to be the same as that of the R410A system, 1.2 kg. (The R410A system uses Emkarate RL68H polyolester as the lubricating oil)

5.3 Charge in the liquid line

Typically, the liquid line linking the condenser to the evaporator is about 8-9 meters long for split systems. The liquid line holds a significant amount of charge (35-45%) in case of a system equipped with microchannel heat exchangers. For the conventional round tube-plate fin geometry, since the heat exchangers have a higher refrigerant side area, the relative percentage of charge in the liquid line is lower (12-15%). For our model, the liquid line diameter is chosen as 6.3 mm (0.2485 inches) [10].

Chapter 6: Off-design performance

On the basis of the simulation model, we have obtained the optimized geometry for the heat exchangers at the design condition (T_{amb} = 35°C, T_{indoor} = 26°C, 50% RH). The next step involves analyzing the system for off-design conditions. The charge in the different components, the evaporator, the condenser, the compressor and the liquid line is calculated and added up at the design condition. This value is then fixed and the model is allowed to run for different ambient temperature conditions, calculating the resulting ΔT_{sub}. The superheat is held constant (5°C), and the rest of the system parameters (compressor size and heat exchanger geometries) are also held constant. The air flow rate over the condenser and evaporator are also kept constant at 2800 and 1200 cfm respectively, as in the design condition, which are typical values for a three ton system.

The system is then allowed to run for off-design conditions. Typically, in case of the conventional R410A round tube-plate fin heat exchanger systems, the condenser charge requirement is greatest at the highest ambient temperature (2.1 kg in this example). At this extreme condition the condenser pressure and 2-phase refrigerant density are highest. The evaporator requires slightly less charge due to its higher inlet quality. The liquid line also requires less charge due to the effect of temperature on liquid density. Hence, with the increase in the ambient temperature, charge moves out of the evaporator and the liquid line into the condenser. The subcooling also decreases slightly with the rise in temperature because the 2-phase region of the condenser requires more refrigerant than the liquid line and evaporator are able to supply, so the subcooled region shrinks.

If R290 were substituted directly for R410A in the same conventional round tube-fin system, the charge distribution would behave differently at off-design conditions. As the ambient temperature increases from 23°C to 37°C, charge would move out of the compressor as well as from the evaporator and the liquid line, to supply the condenser as shown in Figure 6.1.

A significant portion of charge comes from the compressor (~27%) in the R290 case because the oil/refrigerant solubility ratio varies considerably with the ambient temperature, so the refrigerant dissolved in the compressor sump decreases accordingly. In the R410A system, a higher percentage of charge moves out of the liquid line as compared to the R290 system, because the coefficient of thermal expansion for R410A is about 1.8 times greater than that of R290. Also, a higher percentage of charge moves out of the evaporator in the R410A system, since the cycle operates closer to the saturation dome, and thus has a higher variation in inlet quality, as opposed to the R290 system. The overall effect, however in both the systems, is to increase condenser charge about 6-7%, so the off-design performance (e.g. subcooling) does not differ greatly between the R290 and R410A systems when round tube-plate fin heat exchangers are used. For details, including plots of the variation in subcooling at off-design conditions, see Appendix C.
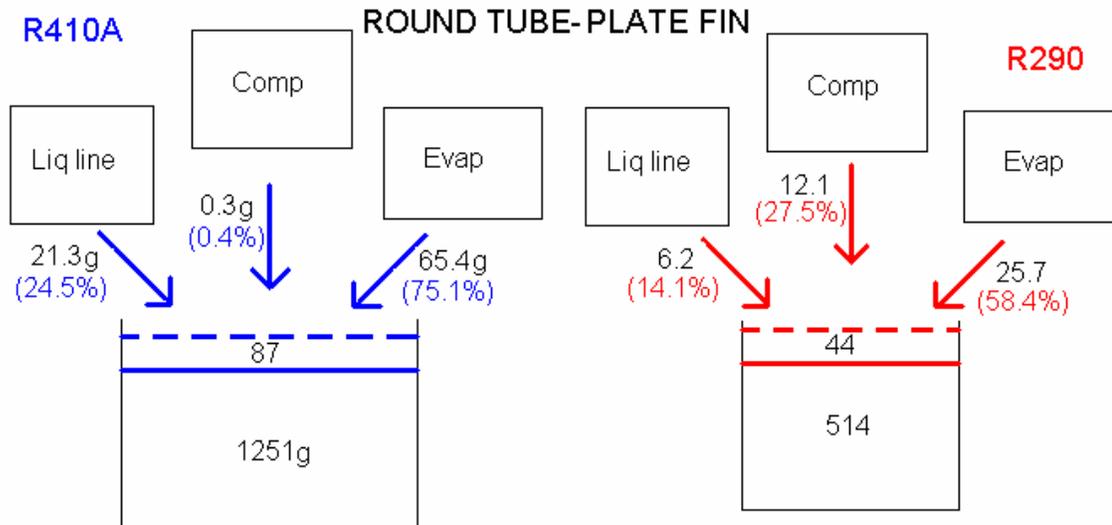
Figure 6.1. Charge moved to condenser from other components in a round tube-plate fin case as T_{amb} increases from 23 to 37°C

Microchannel systems show a very different trend in off-design performance as compared to the round tube-plate fin systems. Figure 6.2 shows that a majority of the charge (~70%) resides in the heat exchangers of conventional systems having round tubes. However, in the microchannels, only about 20% of the total refrigerant charge is present in the heat exchangers.
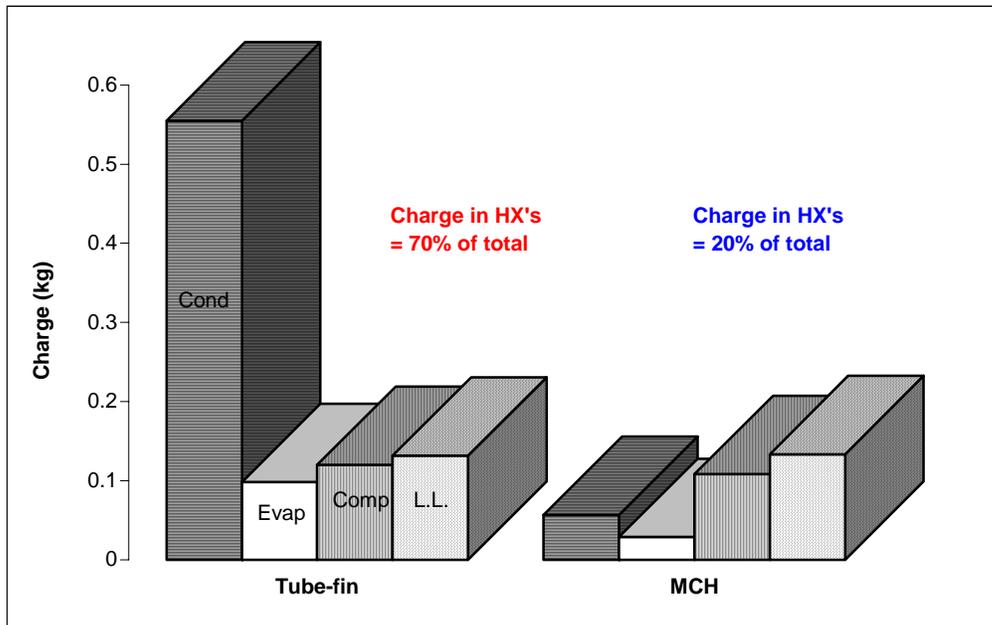
Figure 6.2 Charge distribution for tube-fin and microchannel systems

A typical R410A microchannel condenser requires about 7% more charge as ambient temperature increases from 23°C to 37°C, as it does in conventional systems, if subcooling is to remain relatively independent of ambient temperature. This amount is provided to the condenser by the evaporator, as a result of the change in inlet quality

and the relative volumes of the condenser and evaporator. However, due to thermal expansion, a large amount of additional charge is pushed into the condenser from the liquid line, as shown in Figure 6.3. Hence, with the increase in the ambient temperature, the amount of subcooling increases. This is contrary to what is observed in the round tube-fin systems, where the relative sizes of the components are different. For a more detailed analysis of this phenomenon, including plots of the variation in subcooling at off-design conditions and the difference between the R410A round tube-plate fin and microchannel systems, see Appendix D.


Figure 6.3. Charge moved to condenser from other components in a R410A microchannel case as T_{amb} increases from 23 to 37°C

The properties of R290 exacerbate the situation described above for microchannel systems using R410A. As ambient temperature increases from 23°C to 37°C, charge from the evaporator and the liquid line moves to the condenser, increasing its charge by the ~7% required for holding subcooling constant. This is about the same increase in charge that found earlier for the round tube-fin system with R290. However, at the same time charge also moves out from the compressor and into in the condenser. As a result, the condenser receives a 59% increase in refrigerant mass, when only 7% was needed. (Figure 6.4).

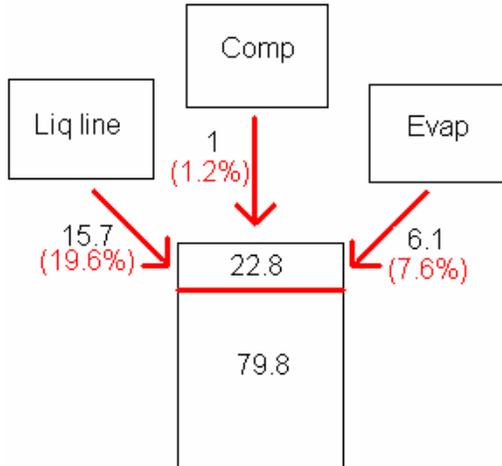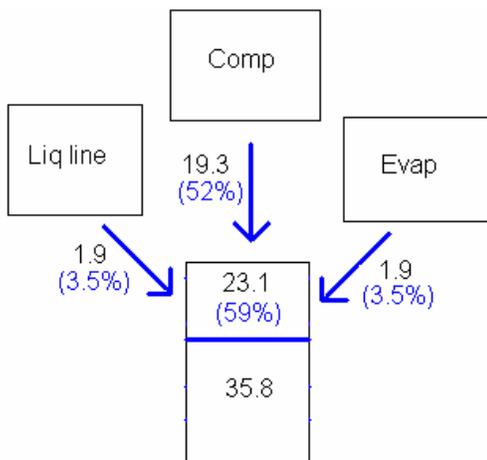
Figure 6.4. Charge moved to condenser from other components in a R290 microchannel case as T_{amb} increases from 23 to 37°C

Since so much additional charge is being pushed into the condenser at higher ambient temperatures, the condenser subcooling increases dramatically. Systems are generally charged to ensure a liquid state at the inlet to the expansion device over their range of operating conditions. Typically, the round tube-fin systems are charged for the hottest day, because subcooling increases slightly at lower ambient temperatures. However, microchannel systems show the opposite trend, as subcooling increases with the ambient temperature. And due to the relatively small volume of the microchannel heat exchangers, such systems will require a different charging strategy as compared to round tube-plate fin systems.

For example, consider a R290 system having optimized heat exchanger geometries shown in Tables 1 and 2. If the system is charged so as achieve a condenser subcooling of 5°C while meeting a 10.5 kW capacity load at the 35°C design condition, subcooling will decrease rapidly on cooler days as shown by the dotted line in Figure 13. Below 30°C, the expansion device may fail to operate properly with a 2-phase inlet. On the other hand if the system is charged to have 2°C subcooling on a 25°C day, the subcooling would quickly become excessive as shown by the solid line in Figure 6.5.
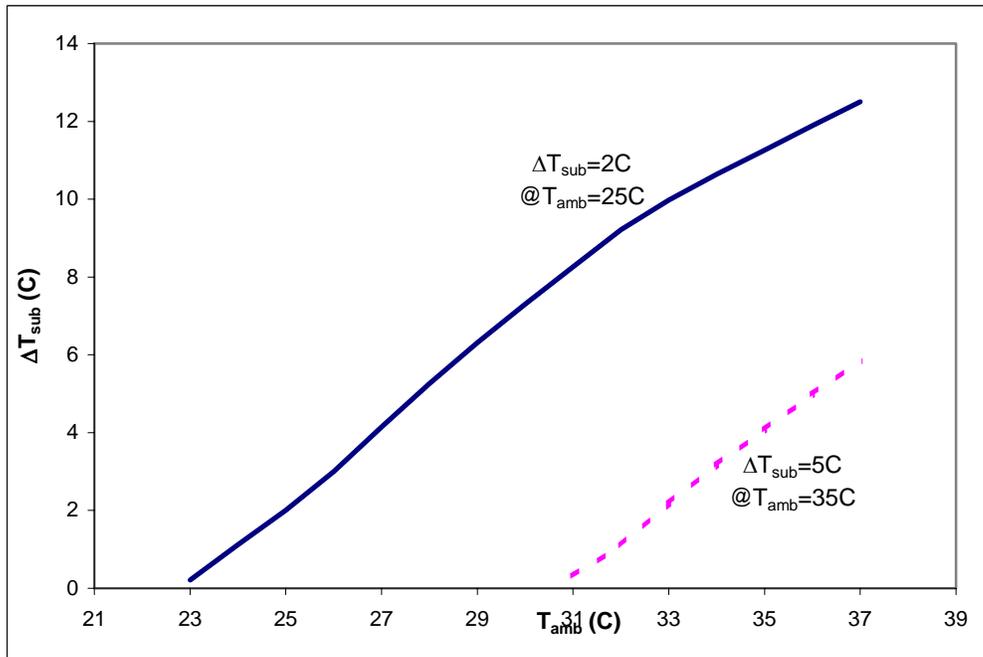
Figure 6.5 Subcooling with varying T_{amb} for R290 microchannel and round tube-plate fin system

Given the shape of the saturation curve, with the rise in T_{amb}, the cycle shifts towards the vapor side, since we are fixing the superheat with the help of the TXV. This would lead to an increase in the inlet quality to the evaporator, and hence a decrease in the Δh and thus a decrease in the evaporator capacity as shown in Figure 6.6.
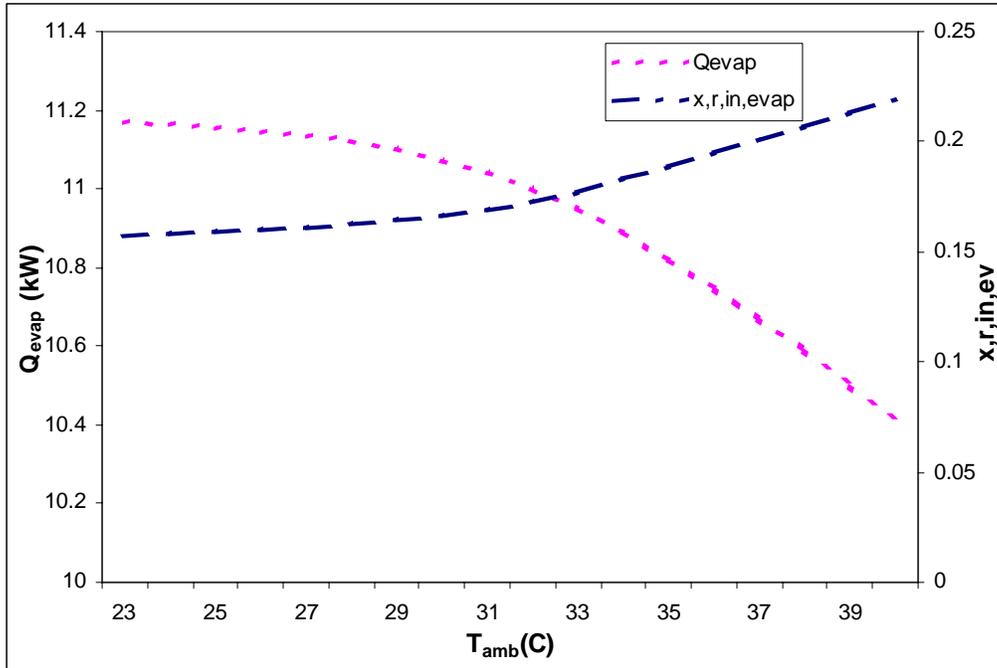
Figure 6.6 Evaporator capacity and evaporator inlet quality at off-design conditions
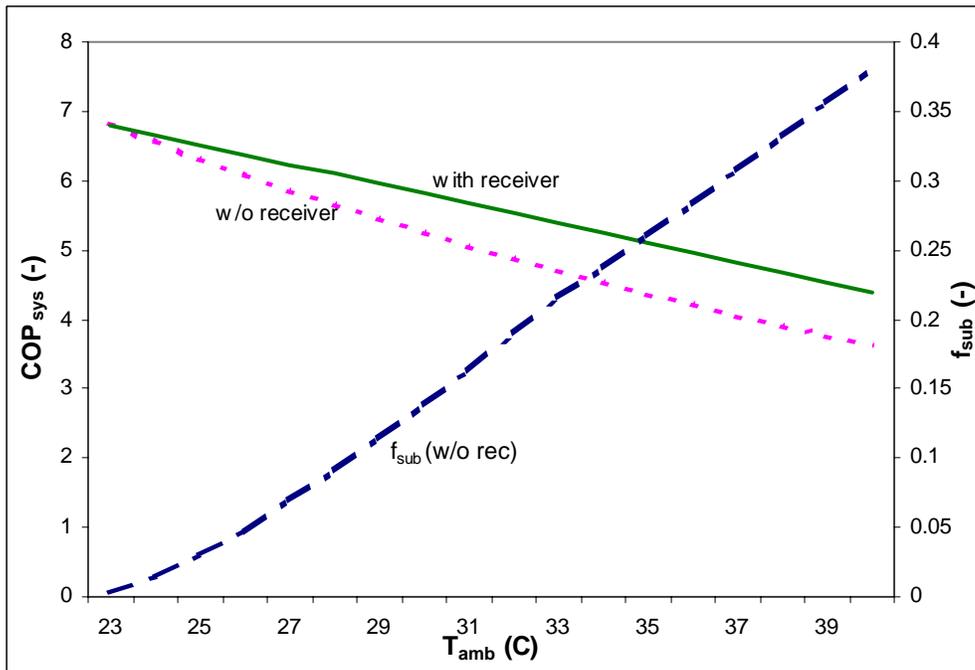
Figure 6.7 System COP and condenser subcooled fraction at off-design conditions

The substantial migration of charge to the condenser degrades its performance by enlarging the subcooled zone to the point where it occupies one-third of the heat exchanger, and forces the condensing temperature upward. The resulting increase in compressor work lowers the system COP as shown in Figure 6.7.

One way of offsetting this problem is to install a receiver at the condenser exit. The receiver would ensure a saturated liquid outlet during steady-state operation at all ambient temperatures, so high system efficiency is maintained. At high ambient temperatures the receiver stores the excess charge, maximizing the size of the two-phase zone of the condenser. The resulting efficiency benefit can be seen in Figure 6.7. In order to prevent flashing in the liquid line, the receiver could be integrated into the condenser along with a small subcooler. Alternatively, the liquid and suction lines could be joined for part of their length to provide enough subcooling to prevent flashing upstream of the expansion device.

Another option would be to use an immiscible lubricating oil, or one in which R290 has a very low solubility. This would not totally eliminate the problem of excess charge in the condenser because of the significant yet smaller migration from the liquid line (Figure 6.3). Reducing the volume of the liquid line would also help. (Appendix E)

Chapter 7: Conclusions

1. By using microchannel tubes, the refrigerant charge in the heat exchangers can be reduced by almost a factor of 5, compared to conventional systems with identical face areas and air-flow rates.

2. Port diameters in the condenser and the evaporator should be reduced to the lowest possible value (e.g. 0.5 mm).

3. The fin height can also be increased by almost 50% of the original value (8 mm) to get a further reduction in charge, but it would increase fan power and reduce the system efficiency.

4. Lowering fin pitch and thickness increases the air-side heat transfer area, thus reducing charge, but also at the cost of an increase in fan power.

5. Refrigerant charge dissolved in the compressor sump varies substantially with the ambient temperature in R290 (propane) systems, but very little in the case or R410A because of the solubility characteristics. This is an important factor for a critically charged system working at off-design conditions.

6. As ambient temperature increases, the coefficient of thermal expansion causes refrigerant to migrate from the liquid line to the condenser.

7. Charge inventory in the evaporator varies by a relatively small amount, due to the operation of the TXV.

8. Round tube-plate fin heat exchangers systems hold almost 70% of the system charge, while this value is around 20% for microchannels. Therefore the migration of charge from the compressor sump and liquid line provides microchannel condensers with far more refrigerant than needed.

9. R290 microchannel systems need to be charged for the lowest operating temperatures. A high-side receiver and/or nearly-immiscible oil is needed to ensure efficient condenser performance at higher ambient temperatures.

References

[1] Granryd, E., Hydrocarbons as refrigerants – An overview, *International Journal of refrigeration*, 24 (2001), 15-24

[2] Hoehne, M., Hrnjak, P.S., 2003, Charge minimization in components and refrigeration systems that use hydrocarbons as a refrigerant, *ACRC*, Project # 141

[3] Park, C.Y., Hrnjak, P.S., 2002, R410A air-conditioning system with microchannel condenser, *Proc. 9th International Refrigeration conference at Purdue University*, paper #R042

[4] Wang, C.C., Chang Y.J., 1997, A generalized heat transfer correlation for louver fin geometry, *International Journal of heat and mass transfer*, 40 (3), pp. 533-544

[5] Dobson, M.K., Chato, J.C., 1998, Condensation in Smooth Horizontal Tubes, *Transactions of ASME, Journal of Heat Transfer*, 120, 193-213.

[6] Incropera F.P., Dewitt D.P., 1996, *Fundamentals of Heat and Mass Transfer 4th edition*, John Wiley & Sons, New York.

[7] Gnielinski V., 1976, New equations for heat and mass transfer in turbulent pipe and channel flow, *Int Chem Engg* 16, p. 359-368.

[8] Souza, A., Pimenta, M., 1995, Prediction of pressure drop during horizontal two-phase flow of pure and mixed refrigerants, In: Katz J, Matsumoto Y, editors. Cavitation & Multiphase flow, New York (NY): *ASME*, FED-Vol.219, p. 161-71.

[9] Wang, C., Kuan-Yu, C., Chang C., 2000, Heat transfer and friction characteristics of plain fin-and-tube heat exchangers, *International Journal of Heat and Mass Transfer*, vol. 43 (2000), p. 2693-2700.

[10] Song, S., Bullard, C.W., 2002, Experimental and Simulation Analysis of Microchannel Evaporators, University of Illinois at Urbana-Champaign, *ACRC* CR-47.

[11] Wattelet J., Chato J., Souza A., Christofferson B., 1994, Evaporative Characteristics of R-12, R-134a and a Mixture at Low Mass Fluxes, *ASHRAE Trans*.;100(1):603-615.

[12] Richter, M.R., Bullard, C.W., 2001, Comparison of R744 and R410A for Residential Heating and Cooling Applications, *ACRC* CR 39

[13] Seeton, C.J., 2002, Solubility, liquid density and liquid viscosity of Witco SUNISO 3GS with Propane, *ACRC*

[14] Private communication with Mr. Wayne Warner regarding the compressor dimensions and lubricant oil charge, August 1997.

[15] DOE/ORNL Heat pump design model on the web, Mark VI

Appendix A: Modifying the system model

The original simulation model used geometry parameters as an input, and in turn calculated variables like the saturation pressure drop and approach temperatures. The model needs to be modified so that these values could be supplied, and hence fixed at a design condition and then the respective geometry variables calculated, ensuring that we get to the optimum geometry. The process of modifying the model involved the following steps.

Changing from 3-pass to single pass

Changing the system from 3-pass to single pass brings the port diameter from 1.3 mm to 0.7 mm, while keeping the other parameters like number of ports, tubes and the frontal area as the same. The original case had an approach temperature $\Delta T_{app}=0.9°C$ and a pressure drop $\Delta T_{sat}=0.27°C$. The change in D_{port} effects these values and they change to $\Delta T_{app}=1.6°C$ and $\Delta T_{sat}=0.46°C$. The charge of the system came down by almost 3 times, since the refrigerant side volume reduced by almost 3 times (down from **0.313 kg** to **0.11 kg**). The depth of the condenser comes down from **21 mm** to **14 mm**, which reduces the condenser fan work. However, since the original case has a lower ΔT_{app}, the discharge temperature is lowered and so is the compressor work. This leads to slightly higher system COP value of 4.93, as compared to 4.8 for the single pass case.

Switching between ΔT_{sat} and L_{tubes}

Next, the pressure drop in the condenser (represented as ΔT_{sat}) is specified as an input. Specifying the pressure drop allows us to calculate the port diameter, as the refrigerant side pressure drop is an inverse function of the port diameter. Since we have the same number of tubes, the D_{port} decreases to 0.57 mm so as to meet the pressure drop requirement. This further helps in reducing the condenser charge and it comes down to **0.072 kg**. The system COP (~4.8) remains fairly unaffected. The condenser depth comes down to **12.5 mm**, which results in the ΔT_{app} increasing to 1.65°C. The step is schematically represented in Figure A1.
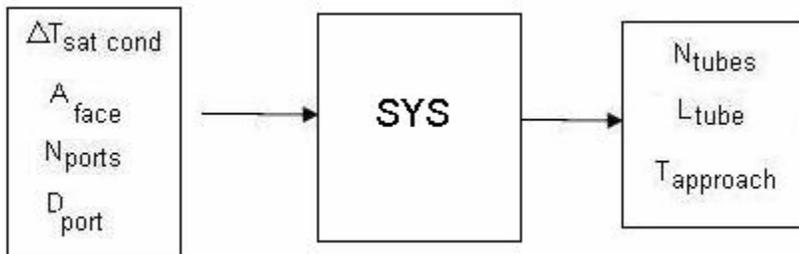

Figure A1. Switching between ΔT_{sat} and L_{tubes}

Switching between ΔT_{app} and N_{ports}

Fixing the ΔT_{app} along with the face area and pressure drop would allow us to calculate the condenser depth, or indirectly the number of ports (N_{ports}). Condenser depth is an indicator of the air-side pressure drop and heat transfer coefficient. The port diameter is calculated as 0.6 mm, while the N_{port} comes out to be 10.4. The depth of the condenser decreases to 11 mm (from the original value of 21 mm), and the three given conditions are achieved. The width of the condenser is approximately 2 m (1.85 m in Park's geometry), while the height comes out to be 0.7 m (0.75 in Park's geometry). The COP falls down to 4.62, since we have a ΔT_{app} fixed as 2°C as compared

to 0.9°C in the base case. The condenser charge goes down slight to **0.068 kg**, because of the reduction in the condenser depth and subsequently in the condenser refrigerant volume. The step is schematically represented in Figure A2.
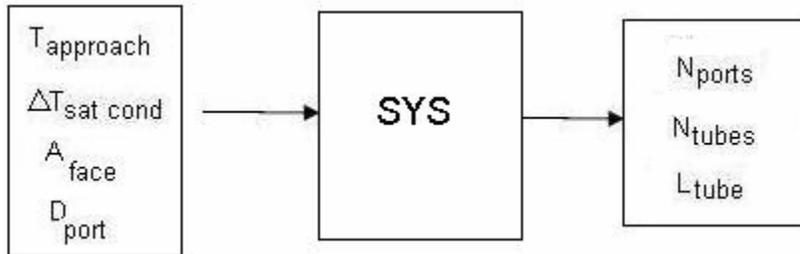

Figure A2. Switching between ΔT_{app} and N_{ports}

Appendix B: Varying fin pitch

In the baseline system, the fin pitch was fixed as 1 mm. Generally the fin pitch is constrained by manufacturing limits and by the condensate drainage considerations. Varying the fin pitch would allow us to analyze its effect on the condenser charge and system efficiency. In the simulation model, the face area and the volumetric flow rate were held constant. Similarly, the refrigerant side pressure drop (ΔT_{sat}) and the approach temperature (ΔT_{app}) were also held constant at 1°C and 2°C respectively, and the fin pitch was allowed to vary from 0.6 to 1.5 mm. The fin thickness for all the cases was fixed at 0.1 mm.

Reducing the fin pitch brings the fins closer, and leads to an increase in the air-side heat transfer area. This would result in shifting the condenser surface area from tubes to fins, and would lead to condenser charge reduction. At the same time, increasing the air side area would allow us to reduce to the condenser depth, thus reducing the number of ports. This would lead to further charge reduction.

However, increasing the fin density would reduce the air flow area, thus increasing the face velocity. An increase in the face velocity would result in an increase in the condenser fan work and hence a fall in the system COP. From the plot it is noted that the benefit of reduced charge obtained by reducing fin pitch is not enough to offset the losses incurred in the system efficiency, and thus the original value of 1mm is used.
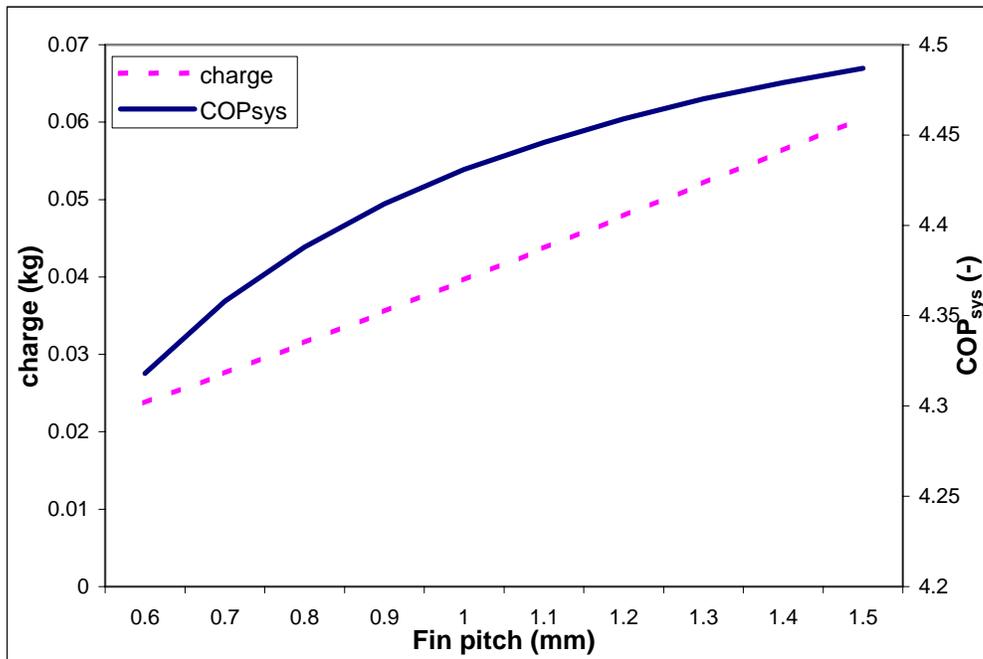

Figure B1. Variation of condenser charge and system COP with condenser fin pitch

Appendix C: Comparison between the R410A and R290 cycles

In this section, we focus on R410A and R290 systems using round tube plate fin heat exchangers, both of which are sized to meet 10.5 kW at 35°C ambient temperature. For both the systems, the charge was initially calculated for the design condition (T_{amb} = 35°C, T_{indoor} = 26°C, 50% RH), and then this value was fixed as constant, and the system allowed to run at off-design conditions. The superheating is held constant (5°C), and the rest of the system parameters (compressor size and heat exchanger geometries) are also kept as the same. The air-flow rate over the condenser and evaporator are also kept constant at 2800 and 1200 cfm respectively, as was in the design condition. Both the systems had round tube standard round tube heat exchanger geometries. The condenser has a face area of 1.4 m², with two circuits each having 10 passes. The first circuit has two modules. The inside diameter of the tubes is 9 mm, and the passes are 1.85 m wide. The evaporator on the other hand has 6 identical modules with 3 rows in the air-flow direction, and has 15 tube passes in the circuit. The tubes have an inside diameter of 8.75 mm and the passes are 0.45 m wide.

With the drop in temperature (from 35°C to 23°C), the subcooling for the R410A system increased slightly (from 5°C to 5.18°C), while that for the R290 system decreased to 3.8°C, as can be seen in the Figure C1.
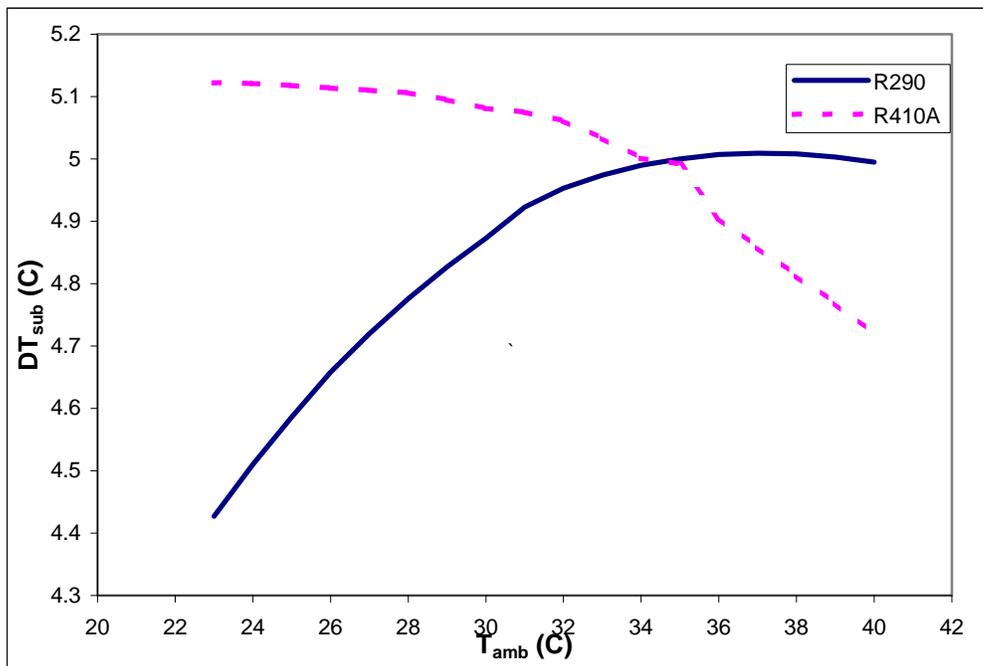

Figure C1. Subcooling with varying ambient for R290 and R410A systems

Next, we analyze the charge distribution in the individual components of the system. With the rise in ambient temperature, the condenser operates at a higher temperature, and is made to reject more heat. As seen in figures C2 and C3, with the increase in operating temperature, the refrigerant density increases, and hence the charge in the condenser also increases. In the R410A system, a higher percentage of charge moves out of the liquid line as compared to the R290 system. This could be attributed to the fact that the thermal coefficient of expansion for R410A is about 1.8 times greater than that of R290. Also, a higher percentage of charge moves out of the

evaporator in the R410A system, since the cycle operates closer to the saturation dome, and thus has a higher variation in inlet quality, as opposed to the R290 system. For the R410A system, the charge in the liquid line and the compressor remain almost constant, since the inlet density to the liquid line and the compressor are almost the same.

A significant portion of charge comes from the compressor (~27%) in the R290 case because the oil/refrigerant solubility ratio varies considerably with the ambient temperature, so the charge within the compressor changes accordingly. The overall effect, however in both the systems, is to increase condenser charge about 6-7%, so the off-design performance (e.g. subcooling) does not differ greatly between the R290 and R410A systems when round tube-plate fin heat exchangers are used.
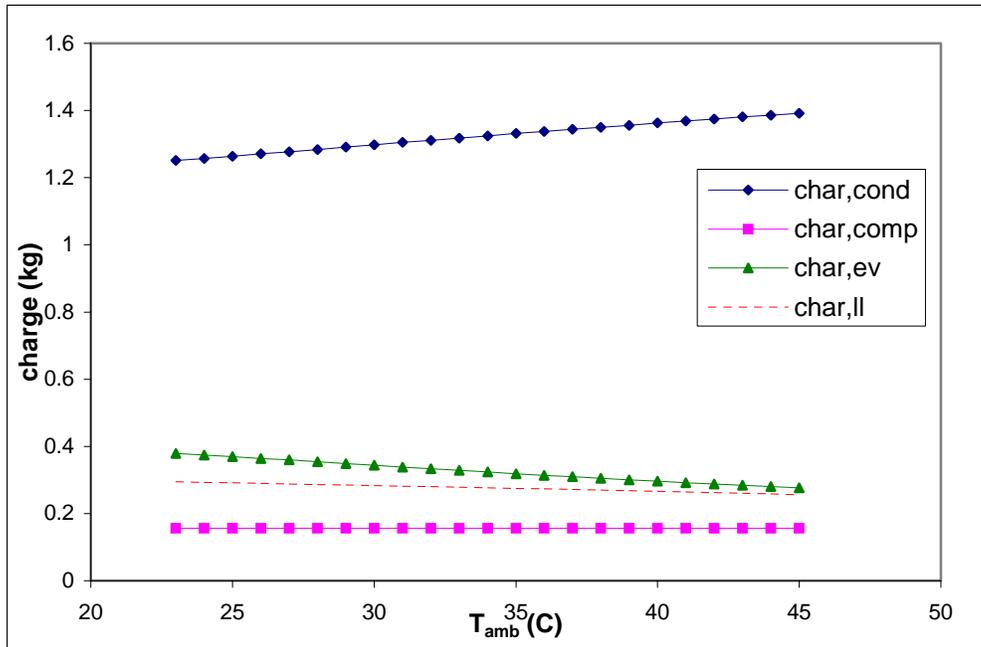

Figure C2 Charge distribution in R410A system for off-design conditions.

However, in case of the R290 system, with the rise in temperature, charge from the evaporator as well as the compressor is pushed out and moved to the condenser. The charge in the liquid line remains almost constant. (Figure C3)

Majority of the charge within the compressor is dissolved within the lubricating oil. The R290 system uses the mineral oil POE32. The refrigerant charge dissolved in the lubricating oil is a function of the oil/refrigerant solubility fraction. This fraction is dependent on the compressor shell temperature. In case of the R290 system, the fraction changes by almost 40% (from 0.07 to 0.05) in the given temperature range (23°C to 45°C). Hence the charge in the compressor shows this variation and decreases with the rise in temperature, as it is pushed into the condenser. The R410A system uses EMKARATE RL68H Polyol ester as the lubricating oil. The oil/refrigerant solubility fraction changes by less than 10% in the given temperature range, and hence the compressor charge is hardly affected. This phenomena governs the difference in off-design behavior of the two systems, and is critical when we are using the microchannel systems, since in those systems the compressor contains almost 30-35% of the refrigerant charge.
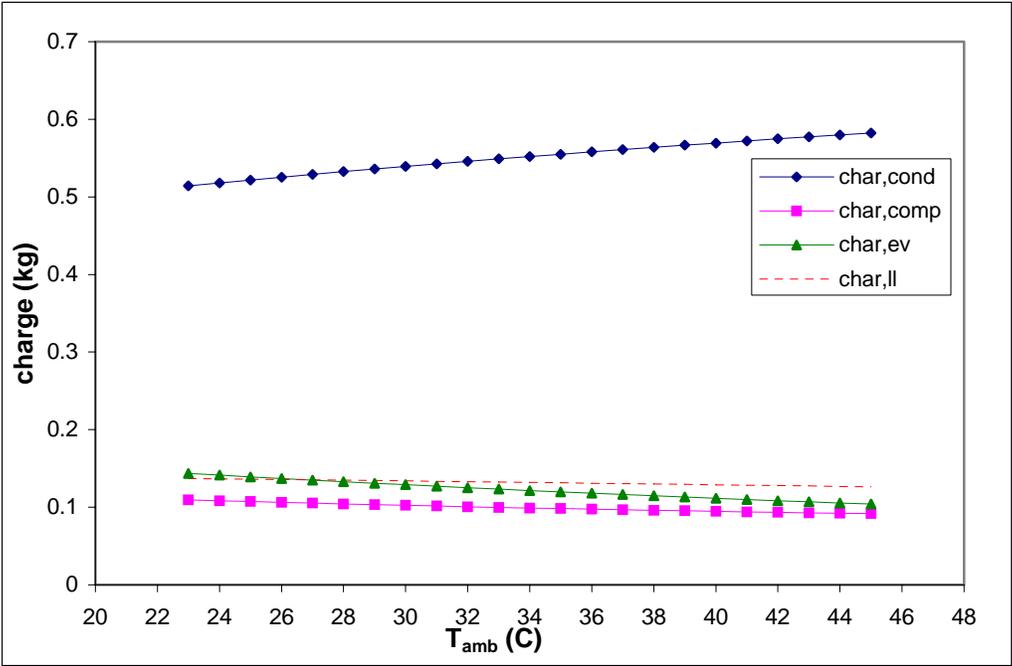
Figure C3 Charge distribution in R290 system for off-design conditions.

Appendix D: Relative distribution of charge in systems with Round Tube and Microchannel heat exchangers using R410A

In the following section we discuss the relative distribution of refrigerant charge in a round tube-plate fin and in a microchannel system, using R410A. Copeland's ZP32K compressor is used for the analysis. The compressor is sized so as to meet the 3-ton load requirement for 35°C ambient conditions. For both the systems, the charge was initially calculated for the design condition ($T_{amb} = 35°C$, $T_{indoor} = 26°C$, 50% RH), and then this value was fixed as constant, and the system allowed to operate at off-design conditions. The superheating is held constant (5°C), and the rest of the system parameters (compressor size and heat exchanger geometries) are also kept as the same. The air-flow rate over the condenser and evaporator are also kept constant at 2800 and 1200 cfm respectively, as was in the design condition.

The round-tube system comprises of a condenser with a face area of 1.4 m^2, with two circuits each having 10 passes. The first circuit has two modules. The inside diameter of the tubes is 9 mm, and the passes are 1.85 m wide. The evaporator on the other hand has 6 identical modules with 3 rows in the air-flow direction, and has 15 tube passes in the circuit. The tubes have an inside diameter of 8.75 mm and the passes are 0.45 m wide.

With the drop in T_{amb}, the condenser saturation temperature ($T_{sat,cond}$) also drops. At lower T_{amb}, the inlet air to the condenser would be at a lower temperature and hence the condenser would operate at a lower temperature.
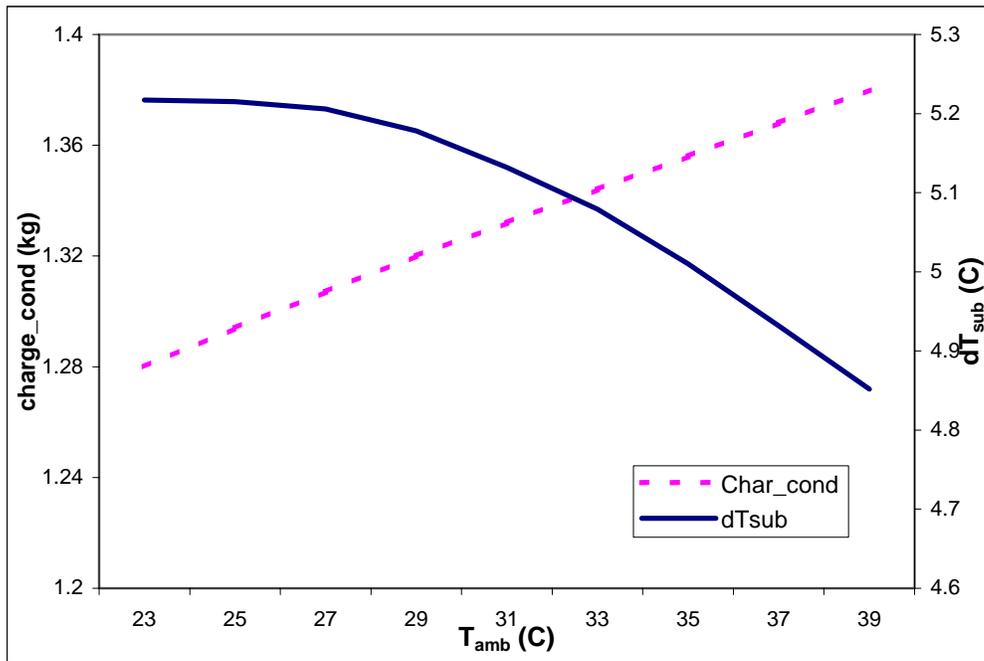

Figure D1. Condenser charge and ΔT_{sub} with changing ambient temperature for a critically charge tube-fin system

With the fall in T_{amb}, the refrigerant density in the condenser decreases, so there is less mass in the superheated phase of the condenser. Since the condenser has to reject less heat and excess charge is available, the sub-cooling goes up, with the drop in T_{amb}. The fraction of condenser area operating in the super-heated also

increases. This is shown in Figure D1. Consider a critically charged system, with increasing T_{amb}. Since the sub-cooling decreases, the cycle should shift, while the superheat is controlled by the TXV. The inlet quality to the evaporator increases with a rise in T_{amb}, as the cycle shifts towards the vapor side. This reduces the Δh in the evaporator, causing the evaporator capacity (Q_{evap}) and thus the COP to decrease. However the decrease in Q_{evap} causes $T_{r,evap}$ to increase slightly, thus increasing the density of refrigerant at the compressor suction inlet and the mass flow rate, but not enough to offset the loss of refrigerant effect. (Figure D2)
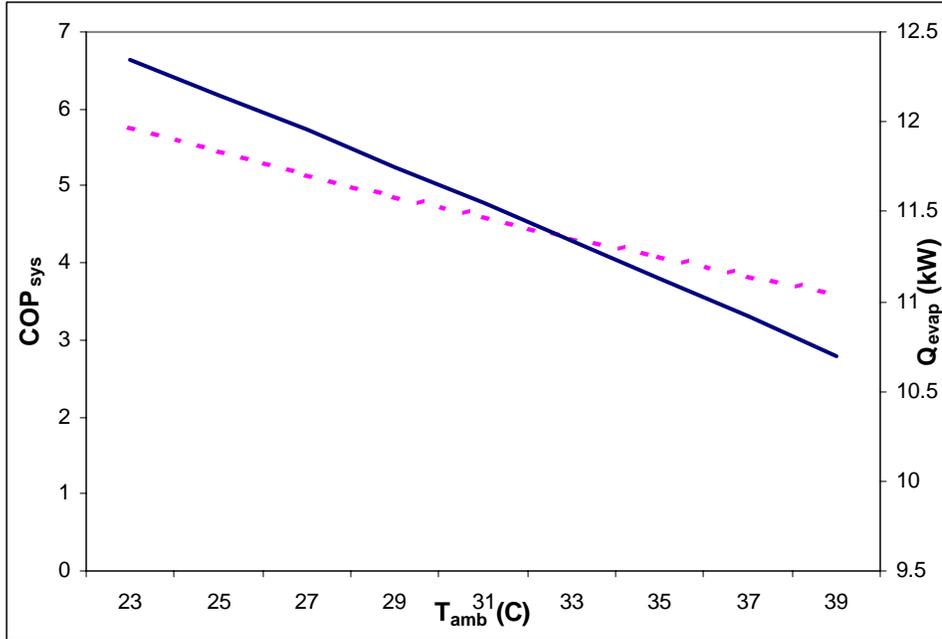

Figure D2. System COP and Evaporator capacity (Q_{evap}) with changing ambient temperature for a critically charge tube-fin system

For the microchannel system, there exist commercial standard geometries for the condenser but none for the evaporator. Hence, we build a simple 3-ton microchannel prototype model with both the condenser and the evaporator having a single pass, single slab structure. The port diameters are assumed to be 0.5 mm for both the heat exchangers, and the fin parameters are chosen from a standard geometry. The tube length and tube depth are calculated on the basis of the ΔT_{sat} and ΔT_{app} constraints. At the design point the saturation pressure drop (ΔT_{sat}) is fixed as 1°C and the approach temperature difference (ΔT_{app}) is held as 2°C, and the parameters are calculated. They are then held constant for the off-design conditions.

In case of the microchannel system, just like the tube-fin case, with the drop in T_{amb}, the condenser saturation temperature ($T_{sat,cond}$) also drops. At lower T_{amb}, the inlet air to the condenser would be at a lower temperature and hence the condenser would operate at a lower temperature. With the drop in T_{amb}, the condenser will have to less heat, and mass is pushed out of the condenser. In the tube-fin case, we noticed with the decrease in ambient temperature the sub-cooling increased. However, for the microchannel case, the opposite is observed, with the sub-cooling gradually decreasing with the decrease in ambient temperature, as in shown in the Figure D3.
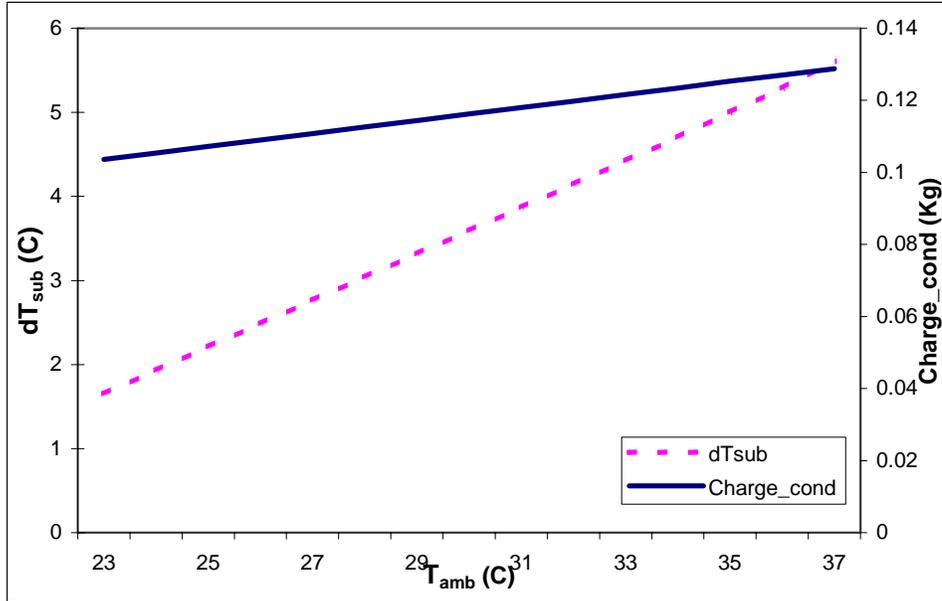
Figure D3. Condenser charge and ΔT_{sub} with changing ambient temperature for a critically charge microchannel system

This can be explained as follows basis. For the round-tube system, the refrigerant side volume is almost four times larger than in the case of the microchannel heat exchangers. Hence in case of tube-fin systems, a majority of the refrigerant charge resides in the heat exchangers as is evident from the Table 1 and Figure D4, which clearly shows that the condenser and the evaporator account for 80% of the charge in the system. On the other hand, in case of the microchannel systems (Figure D5), because of the reduced port diameter and refrigerant side volume, a lesser percentage (20%) of the total system charge resides in the heat exchangers.

Table D1. Relative percentage of charge in different components of a tube-fin and microchannel heat exchanger system

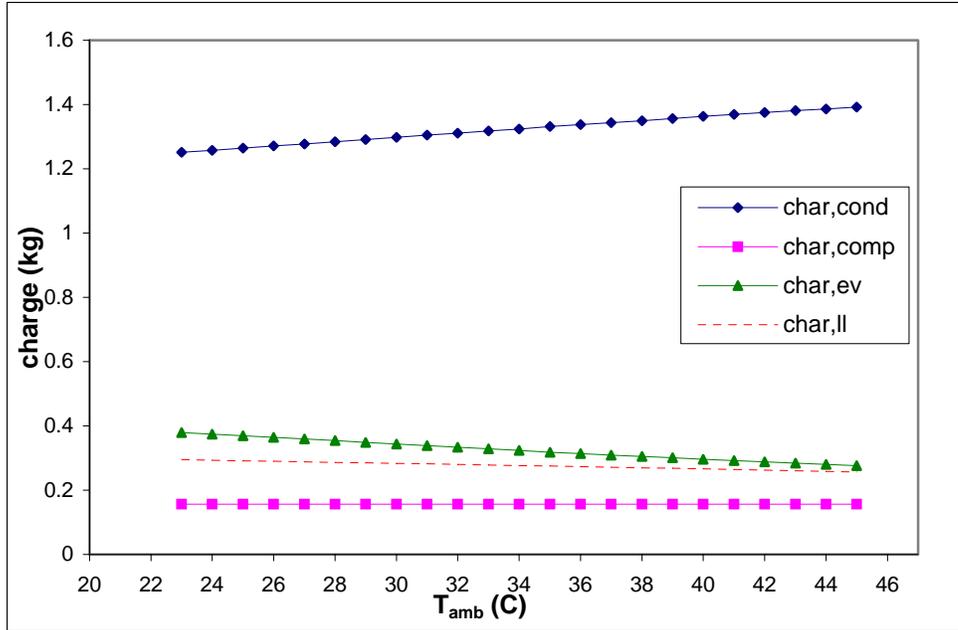| Component	Round tube geometry	Microchannel geometry
Liquid line	13	50
Condenser	65	15
Evaporator	15	6
Compressor	7	29

36

Figure D4. Refrigerant charge in various components at different T_{amb} for Round tube-plate fin system

For the tube-fin system, with a rise in T_{amb}, the condenser needs more charge to reject the extra heat. The increase in T_{amb}, would result in the condenser operating at a higher temperature and thus there is an increase in the refrigerant density, and hence the amount of charge in the condenser increases. Since the refrigerant charge in the system is constant, hence this increase in charge would result in an equal decrease in charge in the rest of the components. Majority of this charge comes from the evaporator. With the increase in T_{amb}, the inlet to the evaporator shifts to a point of higher quality, and thus reduced density, and thus the charge decreases.

However, in the microchannel case, since the refrigerant side dimensions of the heat exchangers have been reduced almost four times, with the rise in T_{amb}, the condenser is not able to pull charge from the evaporator, since it has very low values of refrigerant charge in it. Hence the refrigerant is drawn from the liquid line, and the sub-cooling is strongly affected by refrigerant thermal expansion in the liquid line. With the rise in temperature, the inlet density to the liquid line tends to fall, so as to have reduced charge in it, and the rest could them be sent to the condenser. For the lowering in the inlet density, the system moves to a point of lower $T_{r,cond,out}$ (condenser outlet temperature), which would result in an increase in the sub-cooling with the rise in ambient temperature.

Thus the relative percentage of the charge in the heat exchangers to that of the system governs the behavior of the system for off-design conditions. Even a change in the length of the liquid line would have a significant effect on the off-design behavior of the microchannel system, as can be seen in Appendix E.
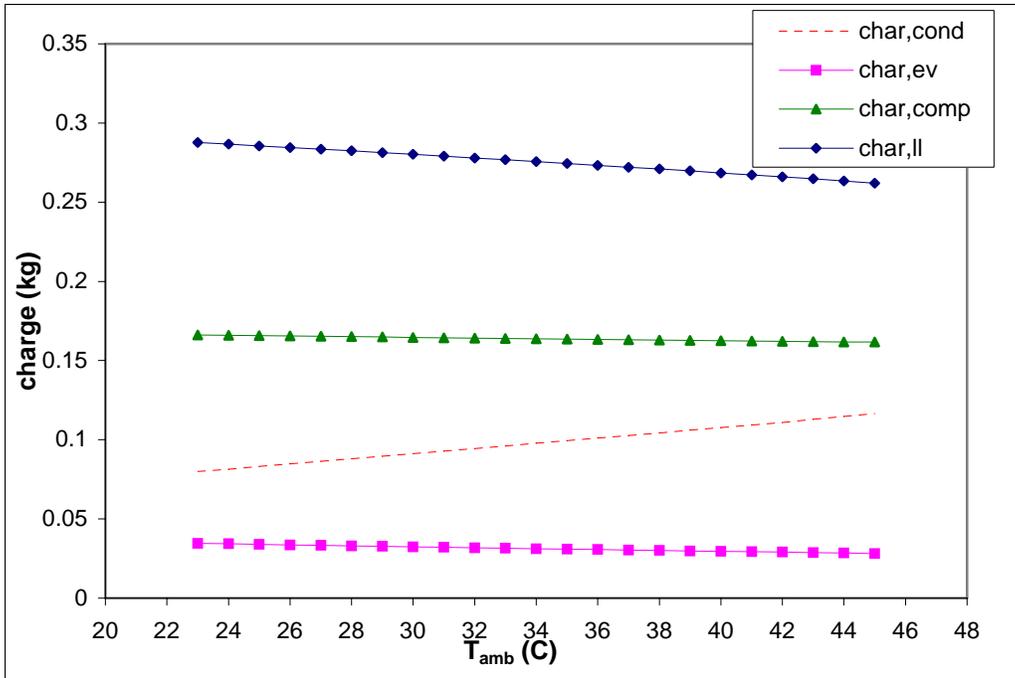
Figure D5. Refrigerant charge in various components at different T_{amb} for MCH system

Appendix E: Effect of the relative size of the liquid line in the microchannel heat exchanger system for off-design conditions

The percentage of the refrigerant charge residing in the two heat exchangers, has a significant effect on these components at off-design conditions, especially on the subcooling of the refrigerant coming out of the condenser. The length of the liquid line determines the charge in it, and depending on the application can vary from about 8-9 m for split systems, to around 1 m for unitary systems. In ultra-compact systems the length of the liquid line would thus decide the relative percentage of the charge in the liquid line and would affect the relative percentage of the charge in the heat exchangers as the entire system. Hence the size of the liquid line would thus determine the subcooling of the refrigerant coming out of the condenser as well.

A simple R410A cross-flow microchannel system with a single slab and single pass structure for both the heat exchangers is used. The port diameters are assumed to be 0.5 mm for both the heat exchangers, and the fin parameters are chosen from a standard geometry. The tube length and tube depth are calculated on the basis of the ΔT_{sat} and ΔT_{app} constraints. At the design point the saturation pressure drop (ΔT_{sat}) is fixed as 1°C and the approach temperature difference (ΔT_{app}) is held as 2°C, and the parameters are calculated. The charge is calculated in the different components and added up at the design condition. Then this value is fixed and the system analyzed to calculate subcooling at off-design conditions. The model is made to run for different liquid line lengths. The results are shown in Figure E1.
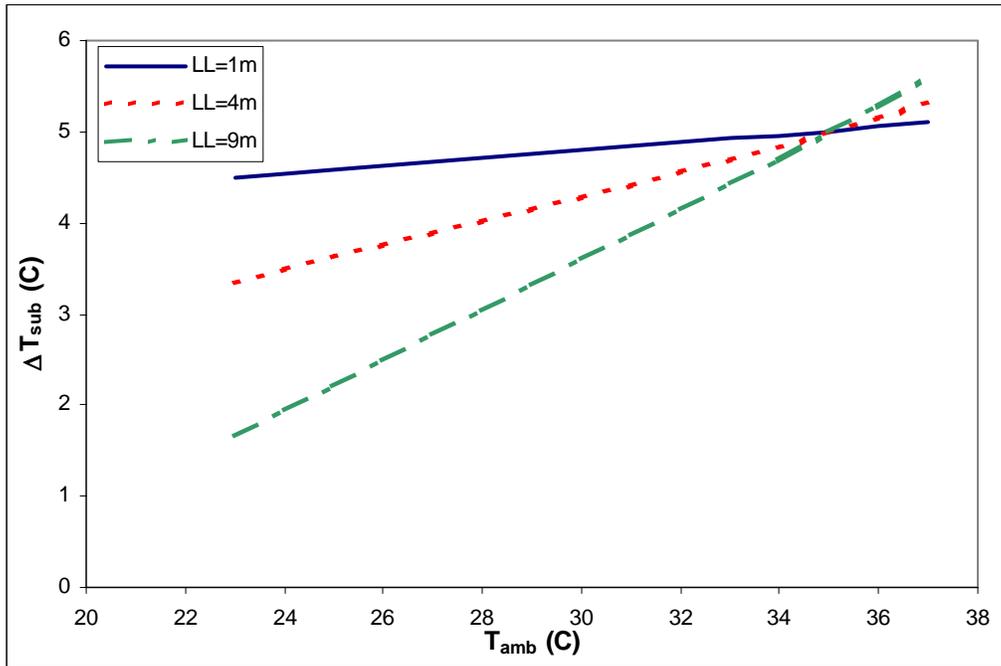

Figure E1. Effect of liquid line length on subcooling at off-design conditions

With a length of 9 meters, the liquid line holds almost 50% of the charge in the system. With the reduction in liquid line length to 4 meters, it reduces to 30%, and finally to about 10% with a liquid line of length 1 meter. With the reduction in length, the relative percentage of charge in the heat exchangers increases from 21% to 44%.

This change is reflected in the slope of the lines in the Figure E1. The increase of relative charge in the heat exchangers tends to make the systems closer to the tube-fin system, where almost 80% of the charge resides in the heat exchangers, as is shown in Figure E2.
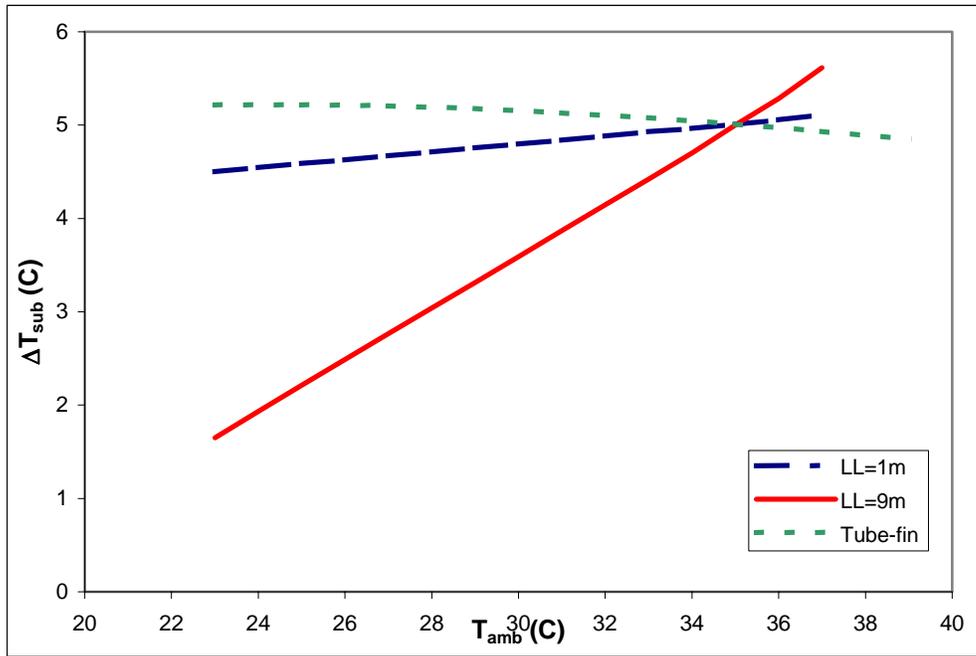

Figure E2. Microchannel vs round-tube system refrigerant sub-cooling response at off-design conditions

Appendix F: Effect of changing lubricating oil in propane based compressors

Air-conditioning and refrigeration systems use a substantial amount of lubricating oil. About 96-97% of this oil charge resides within the compressor sump and is used to lubricate the bearing and piston linings. A small amount of oil flows out to the rest of the system and is returned back to the back. Refrigerants are generally soluble within this lubricating oil, and the solubility changes with the inlet pressure and temperature and it influences the performance or reliability of the compressor as well as the operation of the cycle.

For the microchannel systems, it is observed that around 30-35% refrigerant charge resides in the compressor. The refrigerant charge in the compressor consists of two parts, the vapor, which is present in the compressor shell volume, and the liquid, which is dissolved in the lubricant oil. Since the density of the vapor phase is insignificant as compared to the liquid phase, the refrigerant charge dissolved in the oil assumes a significant part of the total charge in the compressor. The solubility of the refrigerant in the oil would thus govern the compressor charge.

Initially, the mineral oil, Witco SUNISO 3GS was chosen as the lubricant in our system. The following Figure F1 shows the solubility plot for this particular oil.
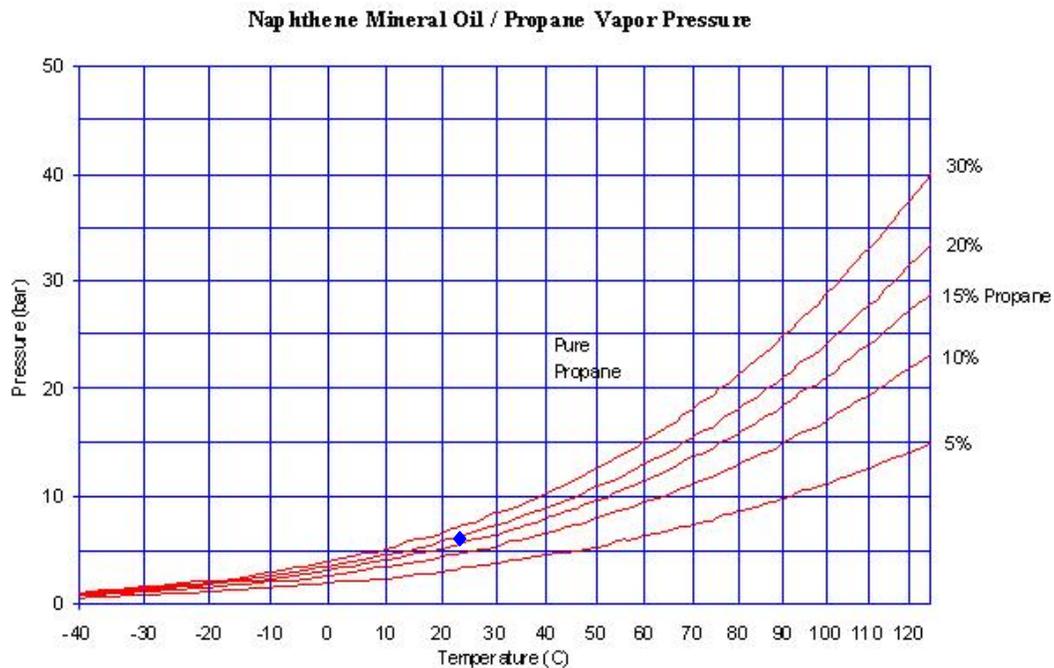

Figure F1. Solubility plots for Witco Suniso 3GS oil / propane mixture

For air-conditioning applications, propane systems generally have suction pressures of the order of 650 kPa. Since typical shell temperatures are in the range of 30-40C, the solubility of propane in this oil is generally around 10-12% (indicated by the point on the plot). And since we are assuming that we have 42 fl. oz. Of oil within the compressor, this amount to about 135-150 gm of refrigerant charge dissolved in the oil. This is a fairly high value, and accounts for almost 35% of the total charge in the system.

Since propane is inflammable, we would want to have the minimum total charge in the system. To reduce the charge in the compressor, we would want to reduce the amount of refrigerant dissolved in the oil, and hence reduce the solubility of the refrigerant in the oil mixture. Thus we choose the lubricating oil such that propane has low solubility in it. After checking the solubility plots for different options, ICI POE (Polyol ester) 32 was chosen. The solubility plots are shown in Figure F2.
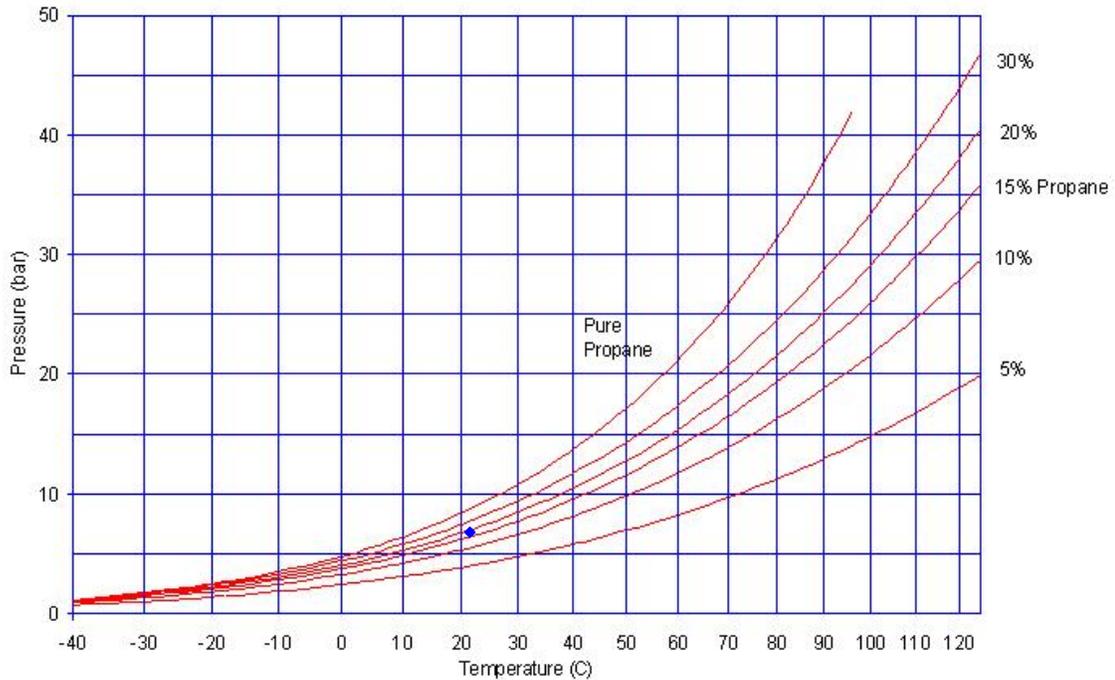

Figure F2. Solubility plots for ICI POE 32 oil / propane mixture

From Figure F2, we notice that the solubility of propane in this oil is around 6-7% at the given suction pressure and shell temperature conditions, which would mean that the compressor charge is reduced to 100-110 gm which and would amount to 24% of the total charge.

Hence, to lower compressor charge, it can be concluded that we need to choose a particular lubricant oil, which has a low solubility with propane. Another option, is to use the relatively new PAG48 mineral oil. The solubility plots are shown in Figure F3. For shell temperatures ranging between 30-40C, the solubility of propane in this oil is around 4-6%. Using this oil, would help reduce the charge in the compressor to about 22% of the total charge. However, the data is still unverified, and needs further testing.
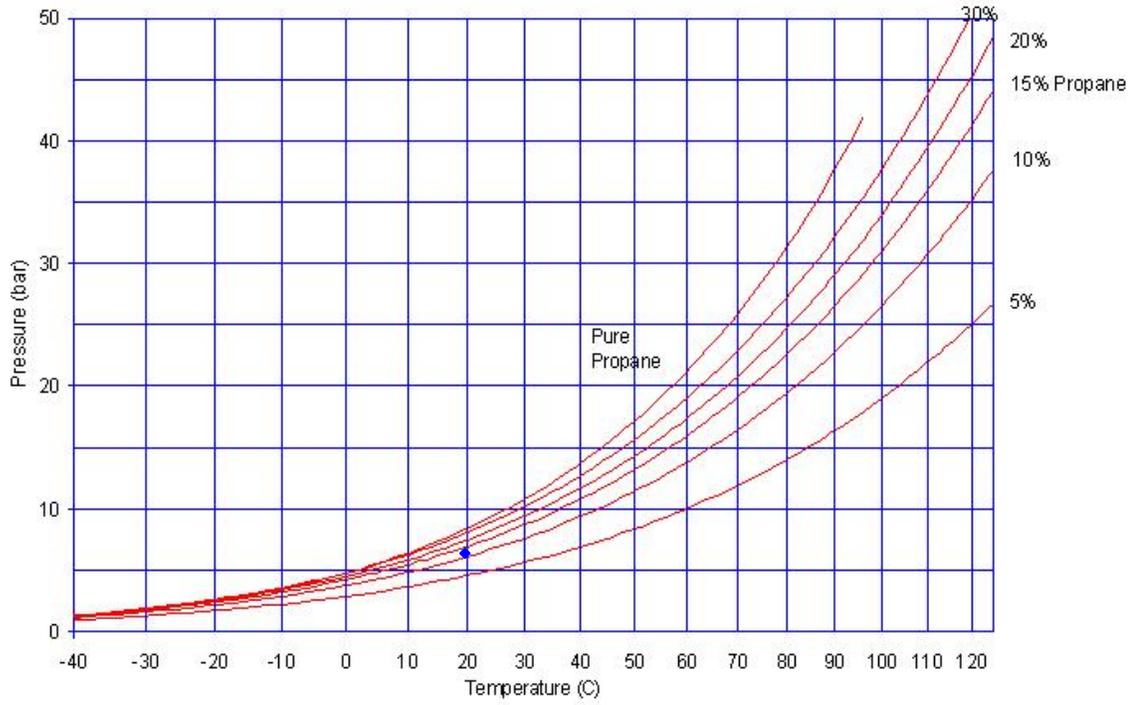
Figure F3. Solubility plots for PAG 48 oil / propane mixture